

CHALMERS



LARGE EDDY SIMULATION OF MIXING LAYERS

Master's Thesis in Applied Mechanics

AMIN LOTFI

Department of Applied Mechanics
Division of Fluid Dynamics
CHALMERS UNIVERSITY OF TECHNOLOGY
Gothenburg, Sweden 2013
Master's Thesis 2013:55

MASTER'S THESIS 2013:55

Large Eddy Simulation of Planar Mixing Layers

AMIN LOTFI

Department of Applied Mechanics Engineering
Division of Fluid Dynamics
CHALMERS UNIVERSITY OF TECHNOLOGY
Göteborg, Sweden 2013

Large Eddy Simulation of Planar Mixing Layers
Analysis of mixing layers and the effects of inlet boundary condition on the
behavior of the flow

© AMIN LOTFI, 2013

Department of Applied Mechanics Engineering
Division of Fluid Dynamics
Chalmers University of Technology
SE-41296 Göteborg
Sweden
ISBN: 1552-8557

Tel. +46-(0)31 772 1000

Reproservice / Department of Applied Mechanics Engineering
Göteborg, Sweden 2013

Abstract

Mixing layers have numerous applications and are of importance in investigations about transition, turbulence and the behavior of different flows in mixing process. Therefore, inquiries about various setups of mixing layers are pretty beneficial. Planar mixing layers are a subset of this subject which are implemented in applications such as combustion furnaces, chemical lasers, the lip of an intake valve in an internal combustion engine and the trailing edge of a turbine blade. Understanding the details of mixing area is critical in terms of chemically reacting and combustion mixing flows.

Here in this project, an investigation on the planar mixing layers in transition to turbulence is carried out both in 2D and 3D. Effects of the splitter plate's trailing edge on the growth of the shear layer is investigated through simulations with different thicknesses of the splitter. Finally, use of an alternative turbulence model (WALE) as a substitute for Smagorinsky model with constant coefficient is put into consideration.

Index Terms: planar mixing layer, transition, turbulence, trailing edge effects, WALE, Smagorinsky

Acknowledgements

This work is carried out at the Division of Fluid Dynamics of Chalmers University of Technology.

I want to thank my supportive and cooperative supervisor Lars Davidson. Weekly meetings with him provided me valuable information for the success of this thesis.

Also, I should thank Shia-Hui Peng for giving advices about the project and all the PhD students of the Fluid Dynamics Division that helped me with the job.

Amin Lotfi
Göteborg, Sweden, 2013

Contents

Abstract	ii
Acknowledgements	iii
Nomenclature	v
1 Introduction	1
1.1 Background	1
1.2 Purpose	2
2 Theory	4
2.1 Governing equations of motion in LES	4
2.2 Turbulence models	4
2.2.1 Smagorinsky-Lilly model	5
2.2.2 Wall-adapting local eddy-viscosity model	5
2.3 Mixing layer in transition	5
2.4 Generating turbulence	7
3 Numerical issues	8
3.1 General setup	8
3.2 Preliminary simulations	9
3.3 Auxiliary simulations	11
3.4 Main simulations	13
4 Results and discussion	16
4.1 Preliminary cases	16
4.2 Auxiliary cases	27
4.3 Main cases	29
4.3.1 Simulation results	29
4.3.2 Comparison of turbulent models	36
5 Conclusion	38
5.1 Summary	38
5.2 Future work	39
Appendices	40
A	41

Nomenclature

Latin symbols

S_{ij}	Rate of strain tensor
W_{ij}	Rate of rotation tensor
C_S	Smagorinsky constant
R	Velocity ratio
L_B	Stream-wise diameter of the bubble
Δ_W	Plate thickness
N_i	Number of cells in i direction
C	Courant number
Q	Second invariant of the velocity gradient tensor
Q_S	Second invariant of the rate of strain tensor
Q_W	Second invariant of the rate of rotation tensor
Re	Reynolds number
B	Two-point correlation function

Greek symbols

ν	Kinematic viscosity
ν_t	Turbulent viscosity
θ	Momentum thickness
δ_ω	Vorticity thickness
δ'_ω	Stream-wise derivative of vorticity thickness
Λ	Wave length
η	Self-similar coordinate
ω	Vorticity
λ	Eigenvalue of the characteristic equation
Δ	Filter width
α	Most unstable wave number

Abbreviations

<i>CFD</i>	Computational Fluid Dynamics
<i>LES</i>	Large Eddy Simulation
<i>DNS</i>	Direct Numerical Simulations
<i>SGS</i>	sub-grid scales
<i>WALE</i>	Wall-adapting local eddy-viscosity model
<i>TDMA</i>	Tridiagonal Matrix Algorithm
<i>RANS</i>	Reynolds-averaged Navier-Stokes equations
<i>CFL</i>	Courant-Friedrichs-Lewy
<i>K – H</i>	Kelvin-Helmholtz instabilities

Chapter 1

Introduction

1.1 Background

CONSIDER two currents with different properties flowing toward the same direction on each side of a finite planar plate. The mixing layer initiates where the flows meet each other at the trailing edge of this plate, starting to exchange momentum and creating a shear layer. *Figure 1.1* demonstrates the setup. This configuration appears in several applications such as combustion furnaces, chemical lasers, the lip of an intake valve in an internal combustion engine and the trailing edge of a turbine blade [1]. In addition, investigations on the behavior of the flow in transitional condition and also in turbulence can be carried out with this setup. Thus, mixing layer phenomena is a significant subject to study.

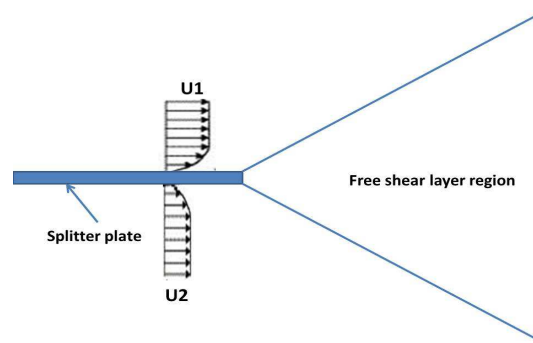


Figure 1.1: A typical planar mixing layer setup.

Early experimental studies of plane mixing layers were performed by Leipmann and Laufer [2]. Many of the statistical quantities were explored in this investigation. Brown and Roshko [3] performed a study on density effects in the mixing layers which lay the groundwork for a virtual revolution in turbulence. Mungal and Dimotakis [4] considered the mixing and combustion of two reactants in a gaseous mixing layer. Later, when the computers' computational speed have started growing and by implementations of new numerical methods,

investigations on plane mixing layers have reached a higher level. DNS and LES simulations of high speed mixing layers [5], particle laden mixing layers [6] and mixing layers with chemical reaction [7, 8] are parts of these investigations.

Although the major focus in the studies on the mixing layers is about turbulent flows, the mixing layers in transition to turbulence are also much studied due to their fundamental importance in practical engineering applications [9]. Transition commence at moderate Reynolds numbers where the pairing of famous Kelvin-Helmholtz (K-H) vortices make the mixing layer grow [10] and at a sufficiently high Reynolds number (based on the vorticity thickness of the shear layer and the velocity difference across the plate) such a pairing interaction would cause the layer to undergo a transition into turbulence [11]. A visualization of this behavior is demonstrated at *Figure 1.2*.

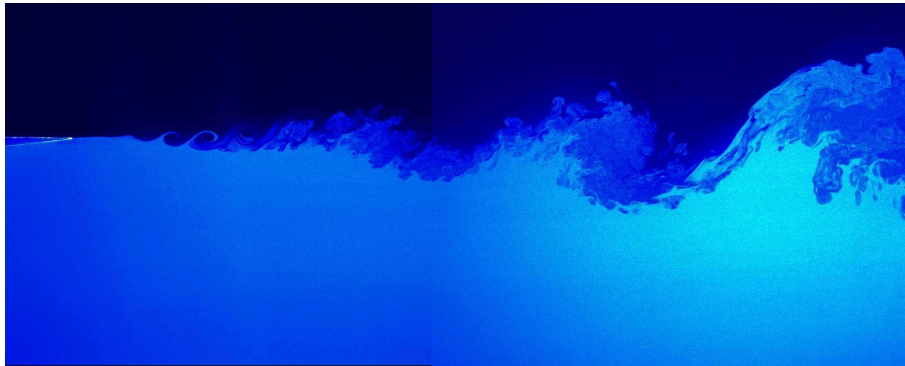


Figure 1.2: Mixing layer visualization [12]

1.2 Purpose

This project is dedicated to an investigation of planar mixing layers in transition to turbulence through two stages; part one, named as *Preliminary stage* consists of 2D and 3D Large Eddy Simulations of mixing layers in a domain which encompasses the growing shear layer excluding the splitter plate. In other words, the inlet of the domain is located slightly downstream of the plate's trailing edge. The domain is large enough to capture the whole mixing layer and its effects on the surrounding flow in all directions. This approach have been used [9, 13, 14] to study mixing layers in transition. The results of the preliminary section are compared to both mentioned previous investigations and also to an experimental result which has a similar setup [15]. The purpose of the simulations is to gather substantial information about mixing layers in transition and also this is considered a mean of validation for further simulations.

Several of the studies conducted about the mixing layers have shown that the growth of the shear layer is sensitive to the initial conditions; experiments with the same setup performed in different apparatus have had a variation in the growth rate by 30% [2]. Some of these inconsistencies are partly related to the splitter plate's trailing edge and the velocity profile in that section [16]. Mc

Mullan *et al.* [13] believe that in order to obtain the behavior of the real flow, the initial conditions must be as close as possible to that of experiments in order to be accurate enough for modeling chemically reacting and combustion flows.

Keeping that in mind, the second round of simulations titled as *Main stage*, are conducted to consider the effects of the trailing edge of the splitter as an active initial condition on the growth of mixing layers. Consequently, the splitter plate should also be inside the computational domain.

To obtain a proper initial condition for the main stage simulations, DNS simulations of the laminar flow on a flat plate is performed. In between, some investigations about a better alternative for the turbulence model used to determine turbulent viscosity in LES equations are carried out. All the simulations of this study are performed by use of Davidson and Peng's [17] CFD code which is written in Fortran language available at Chalmers University of Technology.

Chapter 2

Theory

2.1 Governing equations of motion in LES

LARGE Eddy Simulation is a mathematical model developed by Joseph Smagorinsky which can be used in computational fluid dynamics of turbulent flows. Nowadays this model is utilized in many engineering applications such as combustion, acoustics and simulations of the boundary layers in addition to fundamental research purposes [18] due to its capability to handle large, unsteady turbulent structures and transition. The main idea behind this method is to use spatial filtering in order to narrow the span of resolved length scales which leads to reduction in computational costs. Smaller scales including Kolmogorov scales are being modeled in a proper way using turbulence models (see Section 2.2).

The governing equations can be obtained by implementing filtering on continuity and Navier-Stokes equations. For an incompressible flow with a constant physical vorticity the filtered Navier-Stokes equations results into

$$\frac{\partial \bar{u}_i}{\partial x_i} = 0 \quad (2.1)$$

$$\frac{\partial \bar{u}_i}{\partial t} + \frac{\partial}{\partial x_j} (\bar{u}_i \bar{u}_j) = -\frac{1}{\rho} \frac{\partial \bar{p}}{\partial x_i} + \nu \frac{\partial^2 \bar{u}_i}{\partial x_j \partial x_j} - \frac{\partial \tau_{ij}}{\partial x_j} \quad (2.2)$$

where \bar{p} is the filtered pressure. Reynolds stress terms τ_{ij} which have the basis on the turbulence (fluctuations) of the flow are unknown and have to be modeled.

2.2 Turbulence models

One way to model turbulence is by defining a turbulent viscosity ν_t which can take care of the dissipating energy in a physical manner. In this way SGS scale dissipation occurs like viscous dissipation. This is called *eddy-viscosity* modeling.

2.2.1 Smagorinsky-Lilly model

Assuming that an equilibrium exists between the production and dissipation of the SGS scales, Smagorinsky presented the following Eddy-Viscosity model

$$\tau_{ij} - \frac{1}{3}\delta_{ij}\tau_{kk} = -\nu_{sgs} \left(\frac{\partial \bar{v}_i}{\partial x_j} + \frac{\partial \bar{v}_j}{\partial x_i} \right) = -2\nu_{sgs}\bar{s}_{ij} \quad (2.3)$$

$$\nu_{sgs} = (C_S\Delta)^2 \sqrt{2\bar{s}_{ij}\bar{s}_{ij}} = (C_S\Delta)^2 |\bar{s}| \quad (2.4)$$

where ν_{sgs} is the sub-grid modeled viscosity and Δ as the filter-width is chosen equal to the local grid size

$$\Delta = (\Delta V_{IJK})^{\frac{1}{3}} \quad (2.5)$$

Wall treatment and adjustment of the constant used in equation 2.4 is required since a non-zero turbulence viscosity in the presence of zero velocity is nonphysical while with the Smagorinsky model this happens. The former problem can be solved through setting RANS length scale as a limit for the filter-width (see equation 2.6) and the latter is totally dependent on the flow properties and case geometry [17].

$$\Delta = Min \left\{ \Delta V_{IJK}^{\frac{1}{3}}, \kappa n \right\} \quad (2.6)$$

2.2.2 Wall-adapting local eddy-viscosity model

WALE model introduced by Nicoud and Ducrus is an alternative to Smagorinsky model which is based on the square of the velocity gradient tensor. Calculation of the turbulent viscosity with this model is done using the following equations

$$g_{ij} = \frac{\partial \bar{v}_i}{\partial x_j}, g_{ij}^2 = g_{ik}g_{kj} \quad (2.7a)$$

$$s_{ij}^{-d} = \frac{1}{2}(g_{ij}^2 + g_{ji}^2) - \frac{1}{3}\delta_{ij}g_{kk}^2 \quad (2.7b)$$

$$\nu_{sgs} = (C_m\Delta)^2 \frac{(\bar{s}_{ij}^{-d}\bar{s}_{ij}^{-d})^{\frac{3}{2}}}{(\bar{s}_{ij}^{-d}\bar{s}_{ij}^{-d})^{\frac{5}{2}} + (\bar{s}_{ij}^{-d}\bar{s}_{ij}^{-d})^{\frac{5}{4}}} \quad (2.7c)$$

where g_{ij} is the velocity gradient of the flow and s_{ij}^{-d} is a new-described operator introduced to use in definition of turbulent viscosity. Advantages of this model compared to Smagorinsky model is claimed to be the fact that all turbulence structures relevant for the kinetic energy dissipation in this model are detected, the eddy-viscosity becomes zero at the walls without a need to any adjustments and also this model is able to reproduce laminar to turbulent transition process via the growth of linear unstable modes. The latter comes off due to the fact that the model produces zero turbulent viscosity when only pure shear exists [19].

2.3 Mixing layer in transition

Moving from laminar to turbulence in a flow have several stages and is very complex. Primarily, immeasurable perturbations of the mean status of the flow

start to appear caused by either acoustic or vortical perturbations and according to the nature of the flow these fluctuations can grow or decay spatially. Igniting the primary mode growth, the initial disturbances start to grow following linear stability laws causing secondary instability mechanisms. Non-linearities created after the previous stage with high frequencies and distortion of the mean flow lead to breakdown and finally the flow can be considered turbulent.

In the case of mixing layers, pairing of Kelvin-Helmholtz vortices is acting as the source of perturbation in commencement of transition. It is found that vortex amalgamation and transition is a function of the momentum thickness of the high-speed side boundary layer, θ_1 [11]. It is also noted that the basis of this event is not fixed in a location and has a cyclic path depending on the place that the amalgamation ignites. Another requisite ingredient for the transition to start is stream-wise structures which unfold themselves in plan-view shadow-graph images of the mixing layer that increase the eruptions on the cores of the primary vortices and their intertwined strips [20].

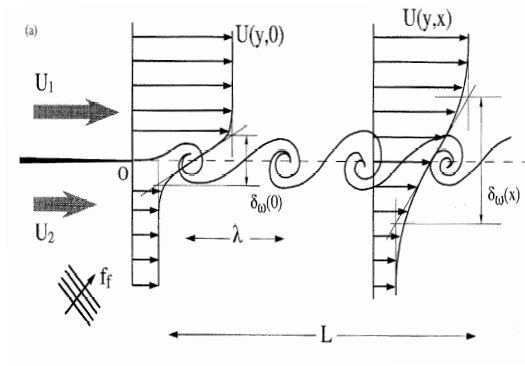


Figure 2.1: Mixing layer setup. The stream-wise velocity profile resembles a hyperbolic tangent function [21].

Getting into details of the pure mixing shear layer, the stream-wise velocity profile in this region resembles a hyperbolic tangent function [22]. Figure 2.1 demonstrates this accurate approximation hypothesis. Taking this into consideration, the stream-wise velocity profile in any cross-section can be evaluated by

$$U(y) = \frac{U_1 + U_2}{2} + \frac{\Delta U}{2} \tanh \frac{2y}{\delta_\omega(0)} \quad (2.8)$$

where $\delta_\omega(0)$ is the initial vorticity thickness of the layer that is calculated by

$$\delta_\omega(x) \equiv \frac{(U_1 - U_2)}{\left(\frac{dU}{dy}\right)_{max}} \quad (2.9)$$

Also, the momentum thickness of the shear layer can be calculated as

$$\theta = \int_0^{L_z} (U_1 - U(y))(U(y) - U_2) dy \quad (2.10)$$

The Reynolds number based on the velocity difference of each side and the vorticity thickness is a pertinent criterion for mixing layer flow property comparison and can be calculated as

$$Re_{\delta_\omega} \equiv \frac{(U_1 - U_2)\delta_\omega}{\nu} \quad (2.11)$$

Another significant factor in the behavior of mixing layers rather than considering the effects of the flow velocity in each side of the plate separately is the velocity ratio that is defined as

$$R \equiv \frac{U_1 - U_2}{U_1 + U_2} = \frac{\Delta U}{2\bar{U}} \quad (2.12)$$

2.4 Generating turbulence

In some applications, the exercised flow is not in the efficient desired state. This can be improved by the powerful multidisciplinary science of Active-Flow-Controls. This fashion has enhanced since the discovery of the boundary layer by Prandtl and mainly focused on the military steady flow systems during the world war [23]. Nowadays this technology has become efficient and is a validated numerical tool for unsteady flow computations at relevant Reynolds numbers. Still, these efforts are too raw for commercial use of the engineering world.

One way to produce proper perturbations as a replacement for the turbulent fluctuations of a flow is to utilize the banded white noise, series of discrete signals with uncorrelated random configurations that have a zero mean and finite variance. In case of mixing layers, the perturbations of turbulence have the same turbulent intensity profile with the banded white noise of equation 2.13 [24].

$$u'(y, z, t) = \sum_{i=1}^{N_f} A \exp(-0.55y^2) \sin\{2\pi f_i t + \phi_i(y, z, f_i)\} \quad (2.13)$$

where f_i is the frequency corresponding to the most unstable wavelength of the mean flow which can be obtained through linear instability theory. For the hyperbolic tangent velocity profile, the most unstable wave number is $\alpha = 0.4446$ [24] and the corresponding wavelength is Λ . ϕ_i is a random independent number and A is the amplitude of the waves which in case of mixing layers is 2% of the mean velocity difference ΔU of the inlet flows. This configuration is due to the homology between turbulent intensity of the created perturbations and the physical fluctuations. For each perturbation a life time is defined and after it is over, a new fluctuation with another random phase and life time is being generated. This insures the flow's realistic properties [14].

This method, although easy to use and cheap to provide compared to making a natural turbulence with a laminar well-described velocity profile upstream with sufficient length for transition to turbulence, it can reach to nonphysical transient and as a result the evolution of the various boundary layer characteristics is not well described by standard empirical relations. This fact is put into test in the current study.

Chapter 3

Numerical issues

ALTHOUGH different series of simulations have been performed in this project, they are all focused on a same matter, the mixing layers. This means all the cases have partly similar numerical setup which is going to be discussed first. Further, separate comments about each case are also included in this chapter. The cases can be divided into three main sections:

- Simulations of the preliminary cases.
- Simulations of the auxiliary cases.
- Simulations of the main cases.

3.1 General setup

As it was mentioned before, all the simulations are performed in CALC-BFC, a finite-volume Fortran three-dimensional code which has specific numerical features. Selected among the options the code offers [17], TDMA algorithm is solving the algebraic relations obtained from the momentum equations, Central differencing is chosen as the scheme to approximate the convective fluxes and fractional step with applied multi-gridding [25] handles the pressure-velocity coupling. The unsteady solver is employed using implicit Crank-Nicolson time differencing scheme for velocities and half-implicit ($C = 0.5$) for the pressure equation. In all cases, orthogonal Cartesian coordinate system with rectangular grids have been used.

Dealing with turbulence, Smagorinsky and WALE methods described in Section 2.2.2 are employed by adding a turbulent viscosity term to the natural viscosity of the flow. Properties of the flow used in the computations are demonstrated in Table 3.1. The Reynolds number is based on the vorticity thickness of the mixing layer which can be seen in equation 2.11 and is chosen to be 700 at the beginning of the shear layer which is considered a moderate number that enables the transition to commence not far from the trailing edge. According to Dimotakis' [26] investigations, one of the requirements for the fully-developed turbulence state is to have a Reynolds number minimum of 10^4 . He also mentions that the transition to turbulence and its length is independent of the flow

geometry. In spite of this fact, the sharpness of the transition according to the Reynolds number is dependent on flow details. The transition for shear layer is considered well-defined.

Table 3.1: Properties of the simulating flow.

Property	Value
Density	1.0
Prandtl	1.0
Viscosity	0.00001
Reynolds Number	700

3.2 Preliminary simulations

The objective of this section's simulations is to obtain a general understanding of the behavior of mixing layers. 2D and 3D simulations have been performed using a rectangular domain. Table 3.2 demonstrates the details of the mesh utilized in the investigations. The wave length is obtained by $\Lambda = 14.132\delta_i$ resulting from linear stability theory. The vorticity thickness can be calculated from equation 2.9 regarding the desired Reynolds number and the properties of the incoming flows. It might come into mind that why the 2D case also has cells in the span-wise direction. This is due to the 3D nature of the CALC-BFC program and it can become easily two-dimensional by isolating (zero convection together with zero high and low coefficients) each cell in this direction. In this way several similar 2D results are obtained and the 2D characteristics of the simulations are conserved.

Table 3.2: Properties of different meshes used for preliminary simulations.

	m	x/Λ		
L_x	0.18	40	case	$N_x \times N_y \times N_z$
L_y	0.061	13.6	2D	$258 \times 98 \times 6$
L_z	0.024	5.3	3D	$258 \times 98 \times 66$

Figure 3.1 demonstrates the domain and the mesh-grids in stream-wise (x) and plate-normal directions (y). It is assumed that in span-wise direction (z), the plate has either an infinite length or is too long that its edges in this direction does not have any effects on the domain. With this in mind, periodic boundary conditions are employed in the xy planes at the boundaries in the z direction. Far from the splitter plate, in cross-stream direction (y), effects of the growing shear layer and the plate are negligible which means all the gradients of the flow can be set to zero, in another words, a free-slip boundary condition is a pertinent setup for this boundary surface.

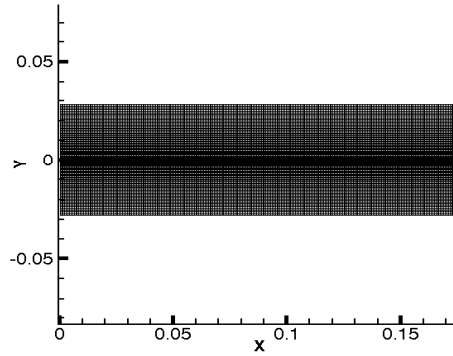


Figure 3.1: xy plane of the computational mesh grid

Commonly, the zero gradient boundary condition is also applied for the outlet plane boundary condition observable at *Figure 3.1*. Previous investigations [27] and preliminary simulations have shown that in a finite length domain, this can affect the behavior of the flow inside the domain in mixing layers. Adding the fact that enlargement of the domain with a consistent resolution requires a lot of more cells, this option is replaced by an effective convective outlet boundary condition with under-relaxations in time as

$$\frac{\partial u}{\partial x} = 0, \quad \frac{\partial v}{\partial x} = 0, \quad \frac{\partial w}{\partial x} = 0, \quad \frac{\partial p}{\partial x} = 0 \quad (3.1)$$

$$C = \frac{Q_{in}}{A} \times \frac{\Delta t}{\Delta x} \quad (3.2)$$

$$u_{new}(ni, j, k) = u_{old}(ni, j, k) - C \times (u_{old}(ni, j, k) - u_{old}(ni - 1, j, k)) + \frac{(Q_{in} - Q_{out})\rho}{A} \quad (3.3a)$$

$$v_{new}(i, nj, k) = v_{old}(i, nj, k) - C \times (v_{old}(i, nj, k) - v_{old}(i, nj - 1, k)) \quad (3.3b)$$

$$w_{new}(i, j, nk) = w_{old}(i, j, nk) - C \times (w_{old}(i, j, nk) - w_{old}(i, j, nk - 1)) \quad (3.3c)$$

$$\frac{\partial p}{\partial x} = 0 \quad (3.4)$$

where Q_{in} and Q_{out} are the inlet and outlet flow rate, respectively. A is the inlet cross-section area. As it is mentioned in Section 2.3, a hyperbolic tangent profile can be fitted as the growing mixing layer's stream-wise velocity. Preliminary simulations have a domain with the inlet is set at a place slightly after the trailing edge of the plate where the mixing layer's growth has already started. This means the hyperbolic tangent profile can be implemented as the inlet velocity profile in the stream-wise direction. Three-dimensional random white noise perturbations with the equation 3.5 are superimposed to the mean

velocities in order to inaugurate turbulence. In consistency with experimental results [24], equation 2.13 is used to provide the requisite banded white noise. Keep in mind that in these set of simulations the effects of the trailing edge of the plate are neglected.

$$u(0, y, z, t) = \frac{(U_1 + U_2)}{2} + 0.5 \tanh 2y + u'(y, z, t) \quad (3.5a)$$

$$u(0, y, z, t) = \sum_{i=1}^{N_f} A \exp(-0.55y^2) \sin \{2\pi f_i t + \phi_i(y, z, f_i)\} \quad (3.5b)$$

$$v(0, y, z, t) = v'(y, z, t) \quad (3.5c)$$

$$w(0, y, z, t) = w'(y, z, t) \quad (3.5d)$$

The simulations have an average time step of 8×10^{-6} and are running for $65000\Delta t$. The variables are time averaged and recorded from 45% of the total number of time steps. Table 3.3 briefly demonstrates the simulations that have been performed with the above mentioned setups. All the cases are carried out in 2D, case A1 and A3 are performed in 3D. Dealing with turbulence, all the cases in this section have been solved using Smagorinsky eddy-viscosity model with a constant coefficient of $C_s = 0.12$. Although the mesh grids are considered coarse in comparison to the previous researches in mixing layers, the results of preliminary simulations agree well with references, hence for this set of simulations there is no need to use a finer mesh.

Table 3.3: Properties of different performed cases.

Case	U_1	U_2	R
A1	31.39	12.96	0.42
A2	21.58	5.19	0.61
A3	32.12	9.59	0.54

3.3 Auxiliary simulations

The hyperbolic tangent velocity is a profile regularly used in spatially developing mixing layers' simulations. Literally, small wake-deficits exist at the inlet of the flow caused by the presence of the splitter which has a major effect on the evolution of the flow and transition locations and is of importance when it comes to modeling of chemically reacting and combustion flows. Thus, a set of simulations containing a fraction of the splitter large enough to cover above-mentioned effects are carried out. These cases are also in need of a proper velocity boundary condition so that the results of the main section could be compared by the preliminary ones.

This section is dedicated to the numerical settings of the auxiliary simulations which have the objective of providing a boundary condition for the main

simulations. The idea is to obtain a stream-wise velocity profile at x_1 , upstream of point x_2 which would have a similar setup providing an initial vorticity thickness of the same size as the preliminary simulations. In this way, both sets of preliminary and main cases have similar settings with a Reynolds number of 700 at the trailing edge of the plate (mixing layer original point). *Figure 3.2* shows this setup.

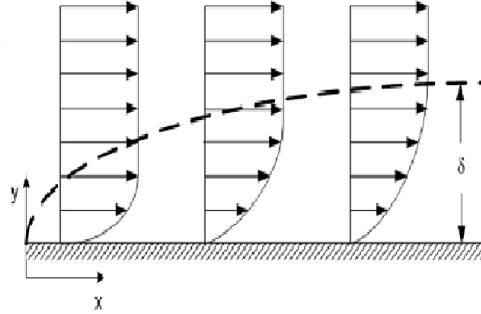


Figure 3.2: Velocity profile at a laminar flow on a flat plate.

Since the definition of the vorticity thickness, δ_ω and Reynolds number based on is somewhat meaningless along the plate, another sort of determination of similarity between preliminary and main cases should be inspected. It has been investigated [28] that fundamental K-H mode frequencies are determined dominantly by high-frequency perturbations which are the results of the formation of vorticity on the fast-speed side of the splitter plate. Therefore, the momentum thickness on the trailing edge of the plate is set to $\theta_1 = \delta_\omega(0)/4$, equal to the inlet momentum thickness of the simulations with hyperbolic tangent velocity profile. For the slower-side of the splitter plate different momentum thicknesses have been suggested due to the fact that the boundary layer of the flow on this side has a low impact on the growth properties of the mixing layer compared to the other side. In consistency with the results of the compared reference [14] $\theta_2 = 2\delta_i/5$ has been chosen for the momentum thickness and the corresponding boundary layer of the lower-velocity zone.

Laminar 2D simulation of the flow on a flat plate has been performed for each side of the splitter plate. The inlet mean velocity for simulations are equal to U_1 and U_2 , respectively. The simulations are laminar since the flows on both sides of the plate from beginning of the plate to its trailing edge stay laminar. This can be investigated using equation 3.6 which indicates that at the highest velocity used in the simulations (32.12ms^{-1}) Re_L is 1.54×10^5 which is less than 10^6 as the recognized border for commencement of transition to turbulence on flat plates [29]. The domain has a $514 \times 80 \times 6$ set of cells and is $.0667\text{m}$ and $.0257\text{m}$ on the stream wise and normal direction, respectively.

$$Re_L = \left(\frac{0.664L}{\theta} \right)^2 \quad \text{Laminar flat plate} \quad (3.6)$$

Since all the domain is located inside the laminar region, no turbulence model

is used, thus viscosity is constant and equal to the natural viscosity of the flow along the whole domain. *Figure 3.3* demonstrates the stretching of the mesh in the normal direction near the wall region. This is vital since small scales should be captured in the boundary layer and as a handy suggestion from the supervisor, at least 30 cells should locate in the boundary zone so that a proper result can be obtained. Settings of boundary conditions can be seen at *Figure 3.3* which indicates that the plate is located upstream of the domain within a small distance to the inlet. The velocity profile at the desired cross-section (x_1) is taken as the inlet boundary condition of the next set of simulations. Uniform flows with velocity magnitudes of U_1 and U_2 are employed as the inlet velocity profile. All other boundary conditions except the no-slip condition at the bottom of the domain functioning as the wall are the same as the preliminary simulations.

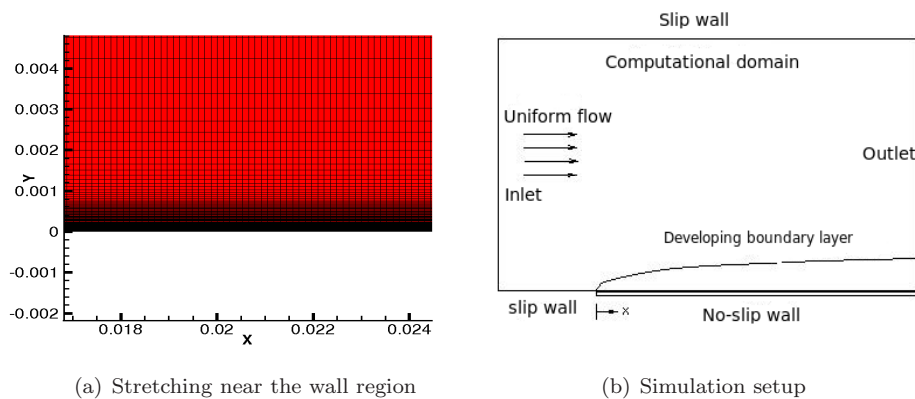


Figure 3.3: Simulation of the laminar flow on a flat plate.

3.4 Main simulations

Obtaining a proper inlet velocity profile from the auxiliary section fully supplies the requisites for the main cases' setup. Here, the effects of different plate thicknesses on the 2D mixing layer are analyzed, one 3D simulation is performed and also an investigation on differences between Smagorinsky and WALE turbulence models is carried out.

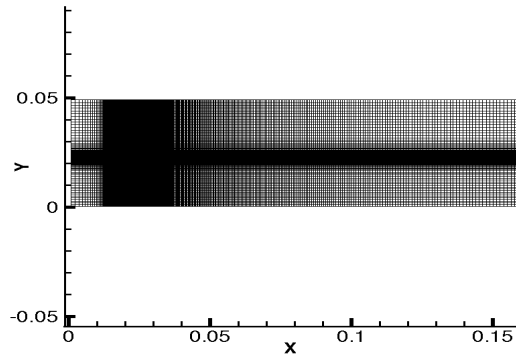
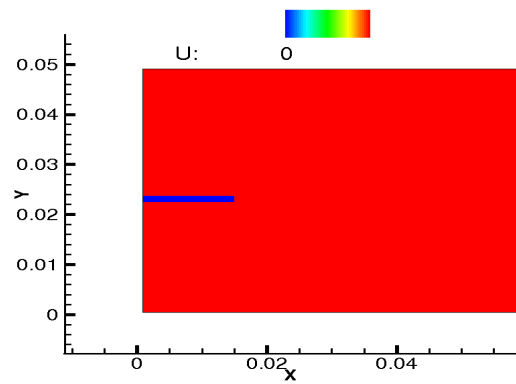
For all cases, the domain is, in consistency with the previous simulations, a rectangular. In the middle of the xy plane of the domain, the plate with 1.5cm length for all cases is located with a number of cells proportional to its thickness depending on the case. *Table 3.4* demonstrates the properties of the domain for different simulations. The flow properties are the same as case *A3* of the preliminary simulations. The cells on the cross-stream direction are stretched in the middle of the domain so that more cells in this direction are located in the boundary layers of the flow on each side of the plate. In order to capture the details of the flow properties where the mixing layer thickness is small, stretching is also employed in stream-wise direction at the trailing edge of the plate.

Figure 3.4 demonstrates the whole mesh for case B2.

Table 3.4: Setup information for main cases.

Case	Size(m)	Size (x/Λ)	$N_x \times N_y \times N_z$	ΔW	Δt
B1	0.167×0.048	33.8×9.8	$706 \times 450 \times 6$	1×10^{-4}	4.45×10^{-7}
B2	0.166×0.048	33.6×9.9	$394 \times 226 \times 6$	3×10^{-4}	6.87×10^{-7}
B3	0.166×0.049	33.6×9.9	$394 \times 258 \times 6$	5.5×10^{-4}	6.87×10^{-7}
B4	0.166×0.049	33.6×10.0	$394 \times 322 \times 6$	1.5×10^{-3}	6.87×10^{-7}
B5	0.169×0.0486	34.2×9.8	$364 \times 226 \times 6$	1×10^{-4}	6.85×10^{-7}
B6	0.167×0.0713	33.8×14.4	$274 \times 192 \times 66$	8×10^{-4}	1.47×10^{-6}
B6	$L_z = 0.022$	$L_z = 4.6$			

At the surfaces of the plate wall boundary condition is employed. Periodic condition in the z on the xy boundary planes, zero gradient on the xz boundary surfaces and a convective outlet boundary is employed to the domain similar to the preliminary cases. Inlet velocity profiles obtained from previous simulations are employed to different cases with a difference in the number of the cells in the cross-stream direction with zero velocity depending on the wall thickness of the case. One can see a sample of this velocity inlet profiles in Figure 3.4. Here, there is no need to add any disturbance such as white noise to the velocity profiles since the trailing edge of the plate itself is a proper trigger for the commencement of turbulence. Smagorinsky model is applied for calculating the turbulent viscosity of cases B1 – B5 combined with a damping in the nearby plate area since turbulence properties should become zero at the wall.

(a) Mesh of case *B2*(b) Demonstration of the the plate near the inlet in case *B2*Figure 3.4: Mesh and the plate in case *B2*.

Case *B1* has a finer mesh for validation of the results in coarser meshes and is compared to the preliminary cases. The 3D simulation *B6* has the coarsest domain in these series of simulations due to its very high cost and the limited amount of time for this study. Using larger cells allows an increase in time steps by decreasing the CFL number, a requisite condition for convergence of PDE equations, which can be calculated as

$$C = \frac{U\Delta t}{\Delta_{min}} \leq C_{max} \quad (3.7)$$

where Δ_{min} is the smallest edge of the calculation cell and C_{max} is considered to have a maximum amount of unity. Keep in mind that higher Courant numbers are not necessarily causing divergence but are indication of a high risk. A bigger time step decreases the number of requisite steps for development of the simulation from its initial condition to its normal unsteady state, reducing the cost of simulations. Case *B5* is performed using WALE model and compared with the Smagorinsky eddy-viscosity model.

Chapter 4

Results and discussion

This chapter is dedicated to the results of all performed simulations and they are displayed in forms of graphs, plots and figures together with some discussions case by case. In consistency with the previous chapter, the results are presented in three sections.

4.1 Preliminary cases

As it was mentioned in Section 3.2, preliminary cases are performed without the presence of the splitter plate. That means the calculation domain in span-wise direction is chosen slightly after the trailing edge of the plate. Provided results divide into two categories, mean flow and instantaneous properties. The former are presented by a self-similar co-ordinate system η which is defined by

$$\eta = \frac{(y - y_{0.5})}{(x - x_0)} \quad (4.1)$$

where $y_{0.5}$ is the location that the stream-wise velocity is equal to the mean of free-stream velocities ($U = (U_1 + U_2)/2$) and x_0 is the origin of the mixing layer which virtually stands upstream of the inlet at the trailing edge of the plate and is not included inside the domain. The growth rate of the mixing layer can be calculated by the vorticity rate formula 4.2 which for this case results into $\delta'_\omega = 0.049$, the lower limit of the correlation [3]. With this in mind, it can be estimated that the trailing edge of the plate is located $0.0061m$ upstream of the inlet boundary.

$$\delta'_\omega = \frac{d\delta_\omega}{x - x_0} \quad (4.2)$$

Literally, a mixing layer does not have an origin with zero vorticity thickness. The minimum possible thickness is the sum of the boundary layer thicknesses of the two sides of the splitter plate and the thickness of it, neglecting the effects of the wake deficits.

Preliminary computations are performed in both 2D and 3D. Starting with the results of two dimensional cases, mean and root mean square (RMS) velocity profiles are demonstrated for the case *A3* in *Figure 4.1*.

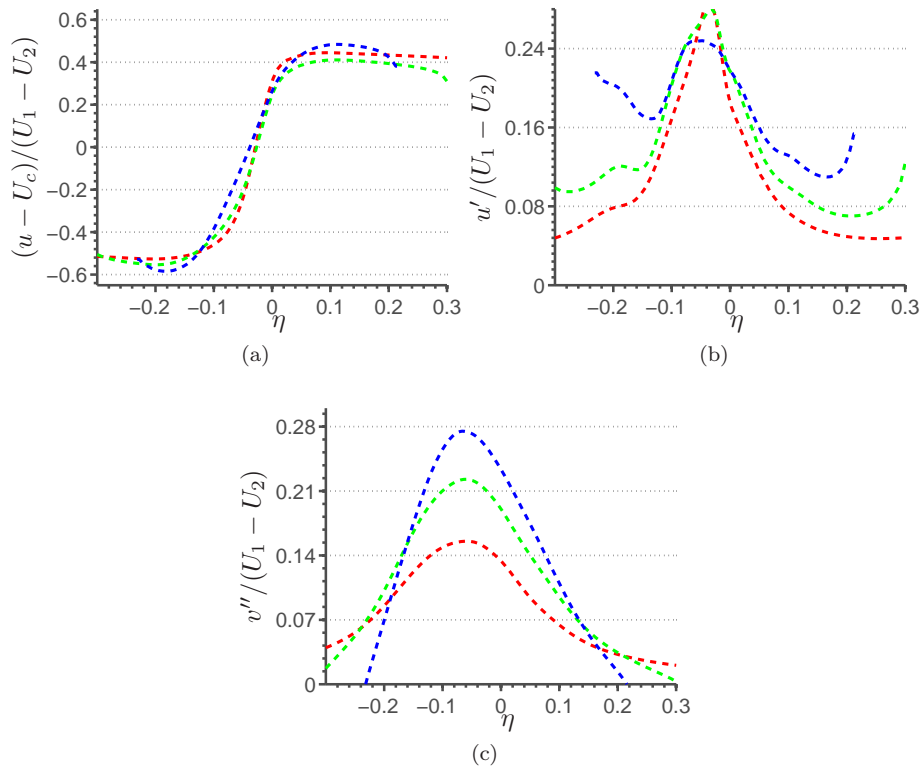


Figure 4.1: Mean and RMS fluctuation velocity profiles for case A3.
 - - - : $x = 0.060m$; - · - : $x = 0.998m$; - - - : $x = 0.1403m$;

The above figures and the results for cases *A1* and *A2* agree well with the previous works that have been performed on the flows with the same properties [3]. It can be seen that maximum fluctuations occur around the zero point of the η coordinate due to the fact that this layer contains all the inflection points for the stream-wise velocity profiles. Large gradient fields in this layer force changes in the instantaneous and mean velocities. The mixing layer's location itself alters in time due to the cyclic movement of the vortex amalgamation. The peak of the perturbations are not exactly at zero coordinate since the mixing layer is not totally symmetric, U_1 and U_2 are not equal. The magnitude and direction of the fluctuations increase as the current flows downstream and this is because of the turbulent mixing activities in the transition area. Self-similarity is a feature of turbulence, the fact that time-averaged velocities in different cross-sections along the stream-wise direction differ in amount and do not fit into each other shows transitional behavior of the flow. Comparing different cases, the mixing layer with a higher velocity ratio (*A3*) has a higher point-wise variance of fluctuations around zero η . In conclusion, a higher velocity ratio results into a thicker vorticity layer and a larger region is affected by high velocity fluctuations.

Figure 4.2 demonstrates instantaneous properties of case A3. Although mean properties of a turbulent flow is preferable in analyzing the overall behavior of the flow, momentary studies are a requisite in analyzing the physical phenomena governing the behavior of the flow and particularly in this case has benefits in inspection of the reacting and chemical mixing of materials and fluids.

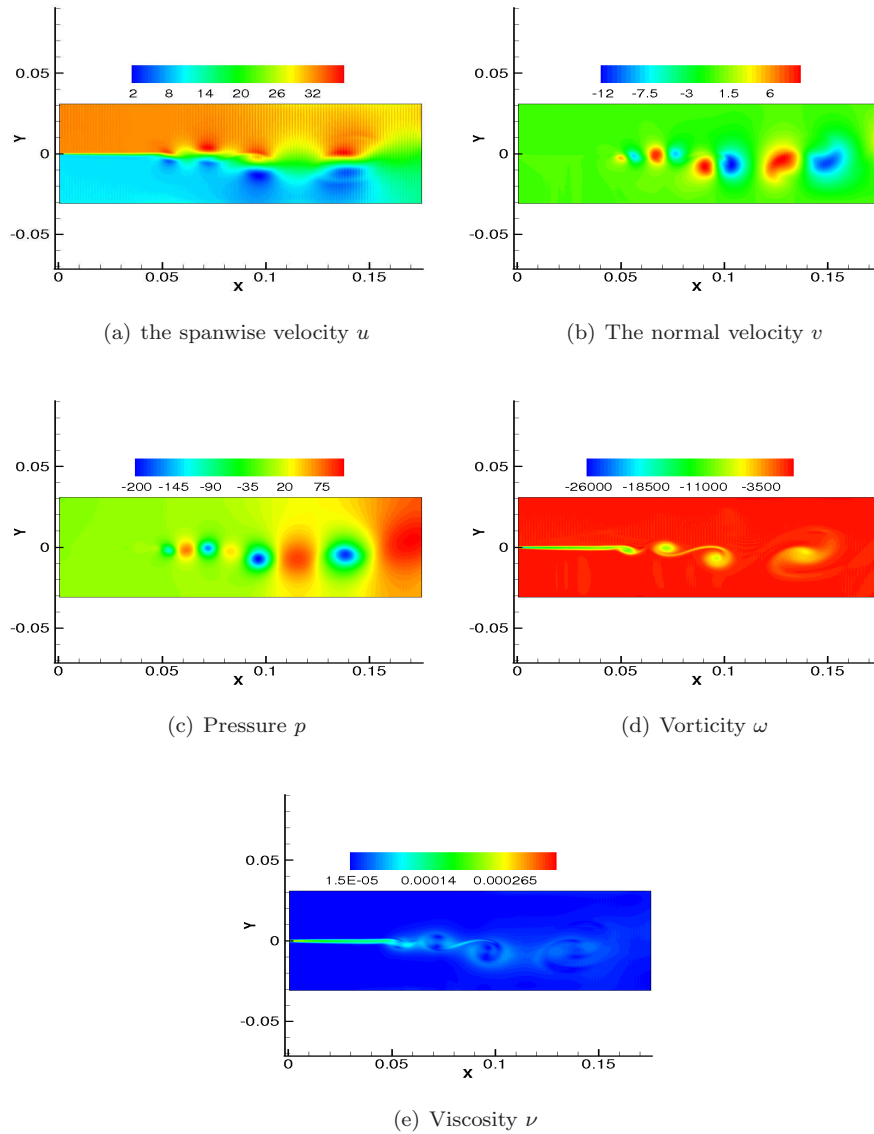


Figure 4.2: Instantaneous properties of case A3 at a specific time.

Getting into details, Figure 4.2 indicates that the transition to turbulence requires a growth in the perturbations of the mean properties of the flow. These fluctuations commence to grow due to the existence of vorticity caused by the

difference in the velocity magnitude and direction of the flow layers at the early stages ($0 \leq x/\Lambda \leq 10$). As the non-linearities start to rise, and the first roll-up of the Kelvin-Helmholtz structures shows up, fluctuations in the mean velocity become visible and raise both in amount and the area they affect; as the flow reaches downstream of the domain, high pressure and velocity gradients are observed. On the other hand, the vorticity and viscosity magnitudes fall down, although they affect larger regions downstream.

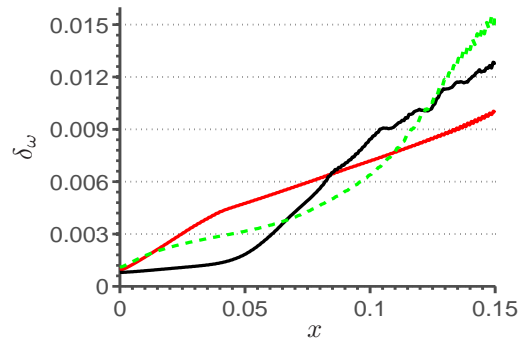


Figure 4.3: A comparison of the vorticity thickness between different 2D cases. — : A1; — : A2; - - - : A3;

The cases for the simulations have been chosen in a manner that a comparison with other researches and investigations become possible. *Figure 4.3* demonstrates the difference between the growth of the shear layer for different inlet velocity ratios. The results agree well with McMullan *et al.* [13] which indicates that higher velocity ratio results into a bigger shear layer and a higher rate of growth which is reasonable due to the fact that a bigger difference in velocities provide higher vorticity fields which are the main source of growth in the vorticity thickness. Non-linearity in growth of the shear layer in 2D cases is a sign of error in the probability of a transition to turbulence and also shows that generation of artificial turbulence might be inaccurate in predicting the location of the commencement of instabilities.

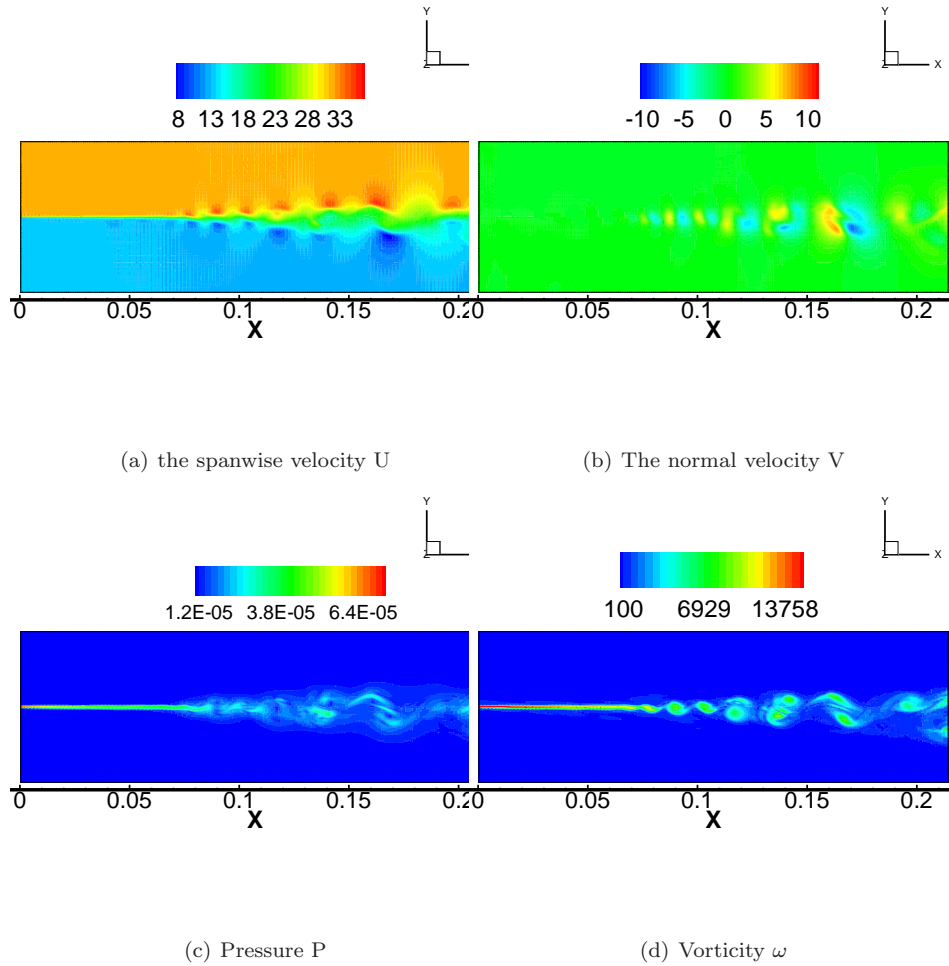


Figure 4.4: Instantaneous properties of the 3D case A3 at a specific time in the mid xy plane.

Analyzing the 3D results indicates that they agree much better with the experimental and DNS in the literature cases which is simply a result of the fact that the transition to turbulence and turbulent flow are 3D phenomena. Comparing 2D and 3D results, *Figure 4.4* shows that the growth trend of the shear layer in 3D result is relatively linear. This more physical behavior is because in vortex tilting process, the vorticity from one dimension transfers into both other directions with the same strength and by disregarding one dimension, a huge amount of interactions are neglected.

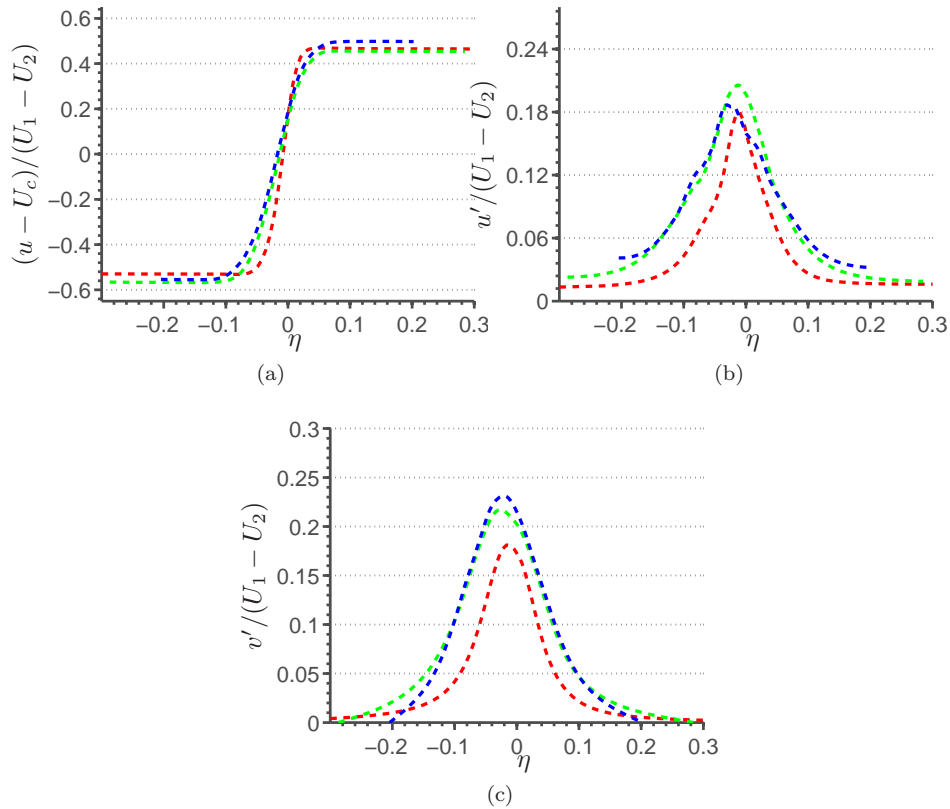


Figure 4.5: Mean and RMS fluctuation velocity profiles A3 in 3D. --- : $x = 0.598m$; - - - : $x = 0.1m$; - - - : $x = 0.1398m$

The time-averaged mean values also agree better with the reference results (look at the appendix A) which can be seen in *Figure 4.5*. The fluctuations in the cross-stream direction have a lower peak compared to 2D case. This is another example of the fact that a large portion of the energy is transferring to the third dimension. Near the trailing edge of the plate and in the transition the results are similar to the 2D cases, the vorticity is limited to a compact area while in the downstream, it is more evenly distributed and uniformly mixed. Since the presence of secondary stream-wise vortices is a requisite for undergoing from transition to turbulence [30], and as in the 2D case these vortices do not exist, the flow is more likely in an unsteady laminar state rather than going into a transition to turbulence [13].

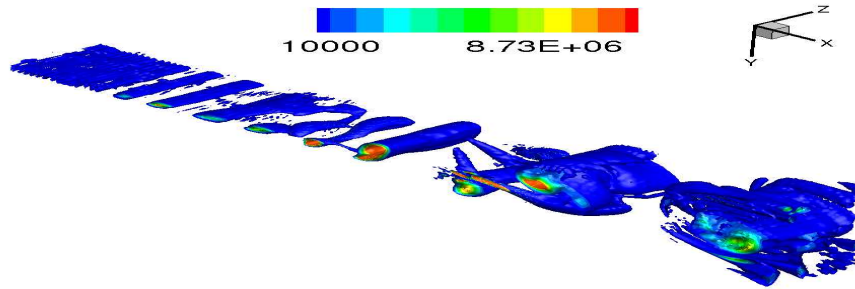


Figure 4.6: Iso surface of high positive numbers of Q . This can visualize small scales in the shear layer.

Generally, turbulent flows include a wide spectrum of scales, some have small velocity gradients (large scales) and much higher vorticity magnitudes occur at small scales. Different methods for identification and visualization of different scales are studied and implemented by researchers. Using invariants of the flow field is an efficient method which can be used in case of mixing layers due to its several benefits; coordinate independence of invariants, ability to bring out the data from 3D to 2D in case of in-compressibility, and its advantages in revealing the features of the flow pattern in space [30]. Consider the velocity gradient tensor, the second invariant of it can be calculated from the characteristic equation 4.3 keeping in mind the fact that in incompressible flows $P = 0$. λ is the eigenvalue of the velocity gradient tensor. A large spectrum of values few Q exists among the domain, large negative values of Q corresponds to the regions where the strain is large and much more effective than enstrophy (this becomes clear expanding the second invariant of the velocity) and in contrast the positive values represent regions with high enstrophy.

$$\lambda^3 + P\lambda^2 + Q\lambda + R = 0 \quad (4.3a)$$

$$Q = \frac{1}{2}(P^2 - S_{ij}S_{ji} - W_{ij}W_{ji}) \quad (4.3b)$$

Figure 4.6 demonstrates the highest spectrum of Q in the domain which visualizes the existence of small-scales concentrated at the shear layer. Notice the concentration of the Kolmogorov scales inside the shear layer indicating that outside this layer only laminar flow exists.

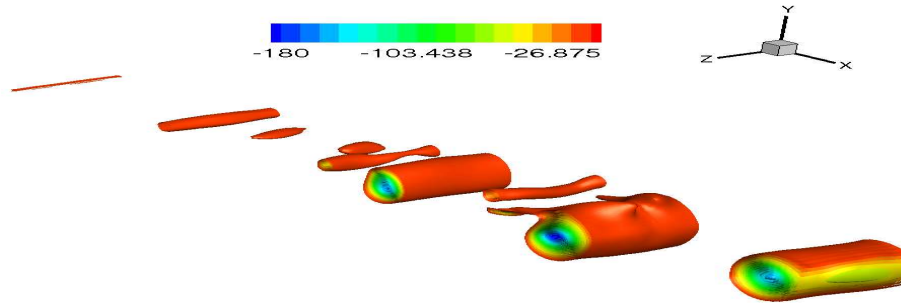


Figure 4.7: Iso surface of pressure in the mixing layer zone. This can visualize large scales in the shear layer.

Lower gradient areas characterizing medium and large scales are often obscured by layers of overlapping points and therefore unreliable to count on in case of shear layers. The roll-up of the K-H vortices is even better detectable by multi (or iso) surfaces of the pressure in three-dimensions which are considered large-scale roller structures of the transitional area that will merge into larger structures downstream [31]. Minimal pressure core lines represent centers of strong vortices which have lower pressure compared to the rotational region around them, providing the requisite centrifugal force which is visible at Figure 4.7.

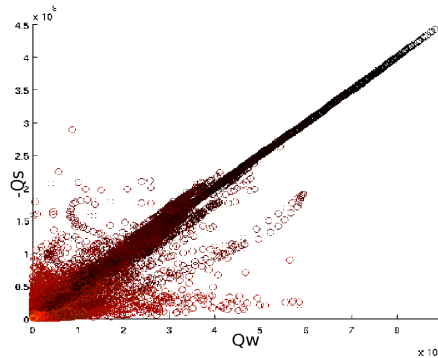


Figure 4.8: $-Q_S$ VS Q_W plot, indication of the behavior of the flow in different cross-sections. Bright red color shows cells which are located upstream and the dark color demonstrates cells in the downstream of the domain.

For a better understanding of the characteristics of the flow in different areas, physical interpretation of various regions can be evaluated through $(-Q_S, Q_W)$ plots. The second invariant of the velocity gradient tensor Q can be divided the rate-of-rotation tensor Q_W and the rate-of-strain tensor Q_S . The points in this figure which are near to $-Q_S$ coordinate are where lower amounts of vorticity exist and irrotational dissipation occurs (large scales). On the contrary, Q_W is a measure of enstrophy density and indicates existence of solid body rotation which occurs near the center of vortex tubes. In the areas where a solid growth happens in the dissipation and enstrophy, a consistency with the physical

picture of a local vortex sheet with dominant velocity gradient within the sheet exists [30]. *Figure 4.8* demonstrates the different cells of the domain belonging to the areas explained. The indication color is darker as the cells belong to a cross-section, downstream in the stream-wise direction. The concentration of the bright points near the origin of the coordinate system indicates that at the trailing edge of the plate no specific structure exists in the flow and transitional properties are in control, also the fluctuations, strain and rotation of the flow are comparably smaller than in the cells downstream. In the upstream part of the domain, the magnitude of enstrophy increases and since most of the cells are concentrated in the mixing layer zone, the figure indicates that local vortex sheets exist in the mixing shear layer area.

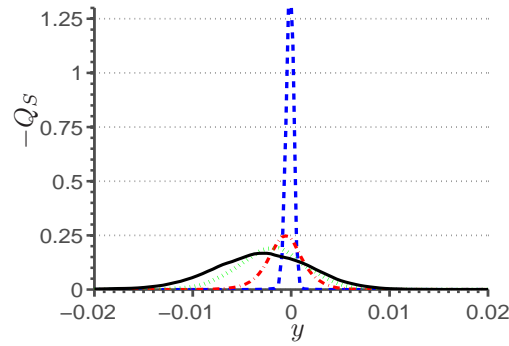


Figure 4.9: Time-averaged rate of strain tensor which is proportional to the mean dissipation of the shear layer. --- : $x/\Lambda = 7.4$; -.- : $x/\Lambda = 14.9$; -.-.- : $x/\Lambda = 22.6$; — : $x/\Lambda = 30.27$

Dissipation of the turbulent kinetic energy is proportional to the time-averaged rate of strain tensor (see equation 4.4). Calculation and comparison of this variable in different cross-sections of the flow indicates (*Figure 4.9*) that dissipation is mostly occurring inside the shear layer where Kolmogorov scale particles exist. Although the area affected by dissipation is expanding, the magnitude of dissipation is decreasing and a more distributed sort of dissipation occurs downstream which is a sign of turbulent behavior.

$$\epsilon = 2\nu \overline{S'_{ij} S'_{ij}}, -Q_S = \frac{\overline{S'_{ij} S'_{ij}} \delta_0^2}{(\Delta U)^2} \quad (4.4a)$$

$$\Rightarrow \epsilon = -2 \frac{\nu Q_S (\Delta U)^2}{\delta_0^2} = C Q_S \quad (4.4b)$$

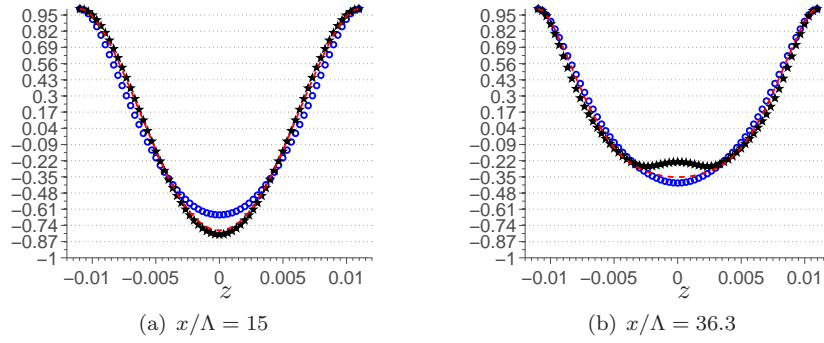


Figure 4.10: Two point correlation function for two cross-sections of the flow. --- : $y = -0.0074m$; ★★ : $y = 0.006m$; ooo : $y = -0.0005m$

Considering the span-wise direction, the domain in this dimension should be wide enough to capture all the shear layer's activities regardless of the dependencies of the flow to the periodic boundary conditions. This factor can be evaluated using a two-point correlation function like equation 4.5.

$$B(z(a), z(b)) = \overline{w'_a w'_b} \quad (4.5)$$

Two point correlation function for w' is calculated in every four cells in stream-wise and cross-stream directions. Figure 4.10 demonstrates the calculations in two different cross-sections of the flow in the stream-wise direction, one in the transitional area ($x/\Lambda = 15$) and another in a more developed turbulence section ($x/\Lambda = 36.3$).

The results indicate that a strong negative correlation exists between the boundary layers of the domain and its center. The symmetry in correlation along the centerline is due to the periodic boundary condition and the approximate symmetry of the growth of the mixing layer in this direction. The correlation curve in the downstream is wider having a lower optimum point and that is because of the existence of a more expansive mixing layer. Figure 4.11 includes the stream-wise cross-sections of the instantaneous velocity contours for a better demonstration of the activities in this direction.

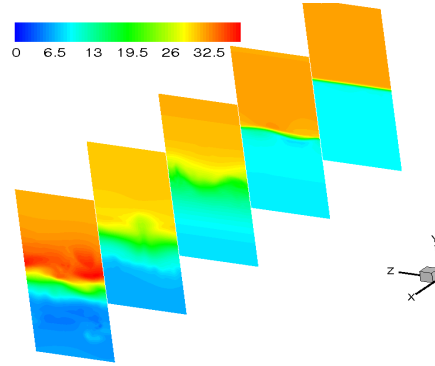


Figure 4.11: Several cross-sectional planes of stream-wise velocity demonstrating mixing behavior in span-wise direction.

For a better comparison of 2D and 3D results, the vorticity thickness and its rate of growth for two cases (A1 and A3) are calculated and demonstrated in Figure 4.12. In both cases, the growth of the shear layer in three-dimensions is far bigger than their counterparts in two-dimension which is reasonable due to the fact that the turbulence growth and vortex tilting are three-dimensional phenomena. According to Brown and Roshko [3], the growth rate of a shear layer is too scattered to be formulated but still, linear growth estimation for the shear layer is pertinent. They mentioned three different ways to fit the experimental data into a linear function using Abramovich-Sabin relation ($\delta'_\omega = 0.181R$), Liepmann and Laufer's [2] lower value of $\delta'_\omega = 0.162R$ which is close to Spencer and Jones' [32] results and also the alternative of using a concave curve that will pass through $\delta'_\omega = 0.175$ at $R = 1$. None of the proposed means of fitting data are more accurate due to the scattered characteristics of the data in this area. The calculated results in 2D (which are marked as blue dots) are not far from this suggestions and in 3D cases (which are marked as yellow dots) they agree well with the above-mentioned proposes.

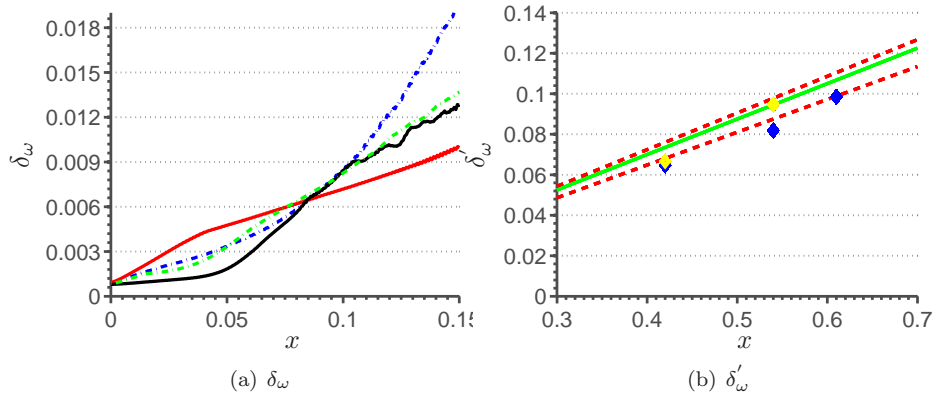


Figure 4.12: Vorticity thickness and vorticity rate of growth for 2D and 3D simulation of cases A1 and A3. — : A1in2D; — : A3in2D; - - - : A1in3D; - - - : A3in3D

Although the vorticity length of the shear layer (δ_ω) is an important fac-

tor in visualization of the mixed area at the presence of vorticity, it can be unreliable due to its definition (see equation 2.9) which is only based on the information from one point. Calculating the momentum thickness is another form of evaluating the growth of mixing layer thickness using all the cells in the normal direction (see equation 2.10). *Figure 4.13* demonstrates the vorticity thickness of cases A1 and A3 along the stream-wise direction indicating a larger thickness (almost twice) in the mixing layer. Flows with higher velocity ratio have a higher shear layer compared to other cases.

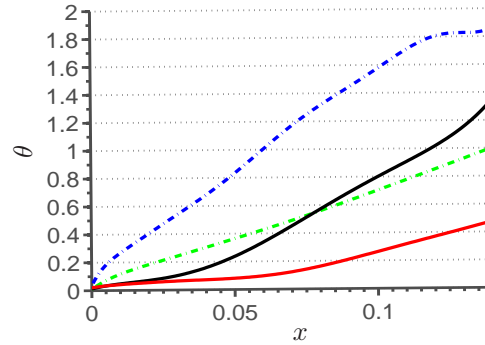


Figure 4.13: Momentum thickness of the mixing layer for 2D and 3D simulation of cases A1 and A3. — : A1in2D; — : A3in2D; - - - : A1in3D; - - - : A3in3D

4.2 Auxiliary cases

Regarding to Section 3.3, auxiliary simulations are performed to provide a pertinent inlet stream-wise velocity profile for the main simulations. First, it is apt to take a look at the calculations which indicate the objectives of this section. Developing boundary layer velocity profile for each side of the plate should be obtained using specific momentum thicknesses ($\theta_1 = \delta_i/4$ for the high-speed side and $\theta_2 = 2\delta_i/5$ at the flank with a lower-speed moving flow). For the A3 case properties into the pertinent equations result into the followings

$$\delta_i = \frac{Re_{\delta_i} \nu}{\Delta U} = 3.1 \times 10^{-4} \quad (4.6a)$$

$$\theta = \frac{\delta_i}{4} = 7.7674 \times 10^{-5} \quad (4.6b)$$

$$\theta_1 = \theta = 7.7674 \times 10^{-5}, \theta_2 = \frac{2\delta_i}{5} = 1.2428 \times 10^{-4} \quad (4.6c)$$

The momentum thickness of a flow on a plate has a different definition and can be calculated by equation 4.7. Now the goal is to find the locations which have equal momentum thicknesses to the above-mentioned magnitudes in each simulation. *Figure 4.14* shows the boundary thickness velocity profiles in the

stream-wise direction. By calculating the momentum thickness in all the cross-sections, the desired location is detected.

$$\theta = \int_0^{L_z} (U_{bulk} - U(y))dy \tag{4.7}$$

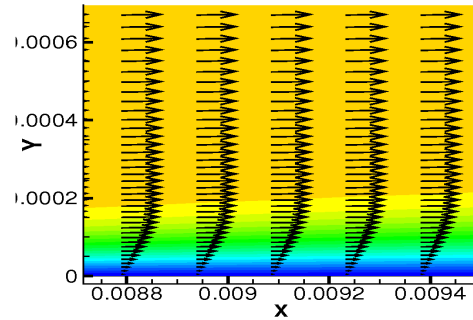


Figure 4.14: Stream-wise velocity profile near the plate. This simulation is done to obtain the B1 – B4 main case’s inlet velocity boundary condition.

1.5cm upstream of this place is chosen as the inlet boundary condition for the main section. The desired profile is created of the two-sides’ velocity profiles plus some zero cells which have zero velocity and no-slip condition on their coefficients in the middle performing the plate’s role. The number of cells with zero velocity depends on the thickness of the plate. Figure 4.15 shows the hyperbolic and the new velocity profile at together.

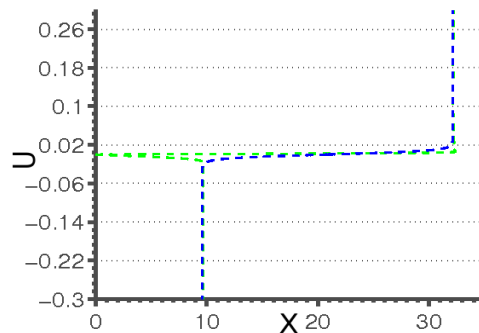


Figure 4.15: A comparison between the hyperbolic velocity profile of the preliminary simulations and the profile obtained from the auxiliary simulations.

Getting into details of the auxiliary simulations, the uniform flow moves forward and it scenes the plate upstream ($Mach \leq 1.0$). The flow starts to move upward near the edge of the plate (Figure 4.16), the pressure increases, the stream-wise velocity drops and vorticity begins to grow in the boundary layer section near the wall. The boundary layer arose will grow as the flow

moves downstream until the flow becomes turbulent and a sudden change in the thickness growth and shape of the boundary layer profile occurs.

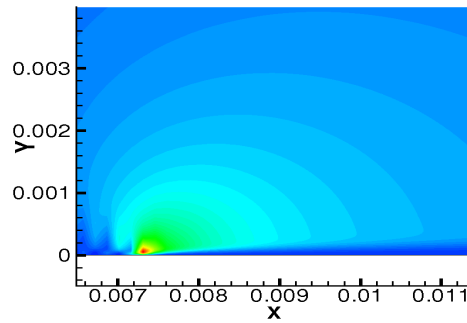
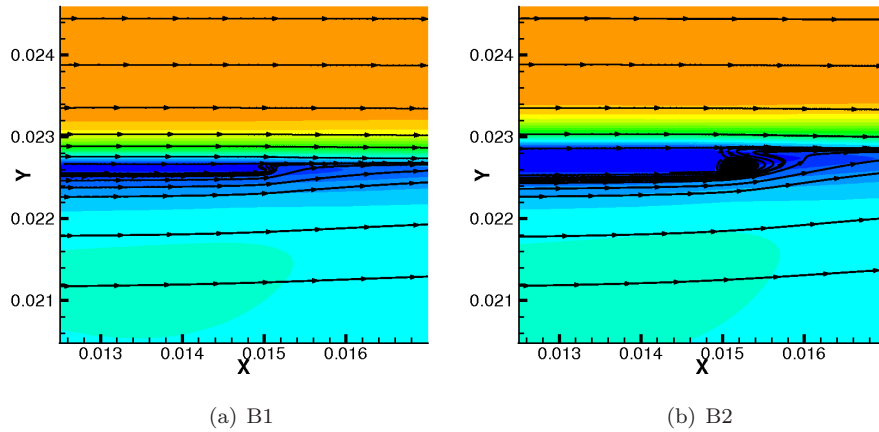


Figure 4.16: The normal velocity of the flow around the edge of the plate.

4.3 Main cases

This section starts with a comparison of the 2D simulations with different wall thicknesses. Then differences of using a hyperbolic velocity profile to a more realistic profile in the growth of the mixing layer is investigated. At last, effects of using another turbulence model to the behavior of the shear layer is considered and described.

4.3.1 Simulation results



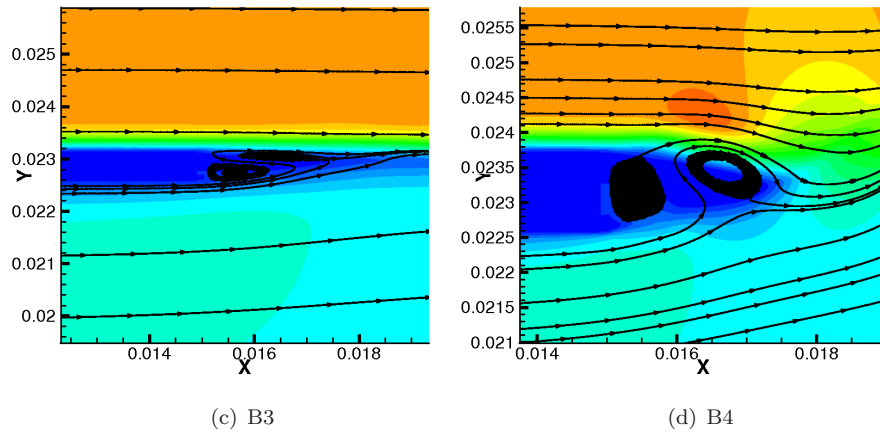


Figure 4.16: The streamlines near the trailing edge for cases B1 – B4

Starting with cases B1 – B4, the first noticeable difference between the preliminary simulations to these cases which have the splitter plate included has its origin in the shear layer’s commencement point where for the previous cases it was assumed to be a virtual single point upstream of the domain. Literally, such point does not exist and the minimum vorticity thickness calculable is bigger than the thickness of the splitter plate. Four realistic plate thicknesses have been chosen for the investigations.

Figure 4.16 demonstrates the trailing edge of these cases. It is clear that in all the cases that when flows from both sides of the splitter reach to the trailing edge, they start to move toward the gap between them due to the existence of low pressure in this zone. High-speed flow, because of the high momentum it has, will not experience much change in its direction and can keep on its motion toward downstream. On the other hand, the low-speed flow will totally lose its stream-wise velocity motion and start to re-circulate to fill in the gap at the trailing edge of the plate. If the plate is thick enough, one or two recirculating vortices are created with low pressure center points near the trailing edge which are fed by the mean stream-wise flows.

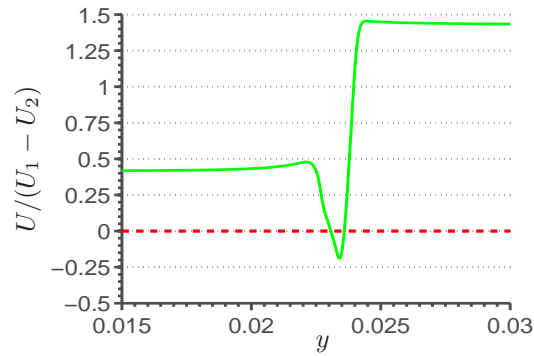


Figure 4.17: Time-averaged stream wise velocity in case B2 at 0.0009m after the trailing edge of the plate which has a single zero velocity point.

The recirculating area forms a bubble at the trailing of the plate. In order to calculate the length of the bubble for each case, time-averaged stream-wise velocity plots such as *Figure 4.17* for case B2 can be drawn for each cross-section of the flow. The plot which has its lowest velocity minimum point at the zero coordinate can be considered as the ending point of the bubble in stream-wise direction. *Table 4.1* includes the bubble lengths for each of these cases. The investigations indicate that the bubble length starts to grow proportionally to the thickness of the plate with an elliptical shape to a specific length, then the bubble starts to shape a circular form as the plate gets thicker and it shrinks in stream-wise diameter. This can be due to the fact that the source of the vorticity and as a result, shape of this bubble is dependent on the speed of the flows moving toward the edge of the plate which are constant. The diameter of the bubble in y direction is dependent on the thickness of the plate, so that the stream-wise diameter of the bubble is a variable of ΔW , U_1 , U_2 and the low pressure field after the trailing of the plate.

Table 4.1: Bubble length for different cases.

Case	$L_B(m)$
B1	0.00016
B2	0.0009
B3	0.0026
B4	0.0020

The comparison of the results of the new setup with the preliminary simulations is deferred until after the presentation of the 3D result. Getting into more details of the differences caused by the thickness of the plates, *Figure 4.18* demonstrates vorticity and momentum thickness for each case as an estimation of the mixing layer growth. It is obvious that there are differences in the pattern of growth in the vorticity thickness near the trailing edge of the plate. Simulations with thinner plates show smoother curves whereas the thick plates have an abrupt growth which is due to the effects of the low pressure field and the big

gap between the flows downstream of the splitter which creates additional gradients and perturbations to the mixing layer which are damped through space down stream and at the end when the flow is becoming turbulence, the shear layer thickness for all cases diverge to same magnitudes. This is because the turbulent condition is negligibly unaffected of the plate-caused deficits in contrast to the transitional area.

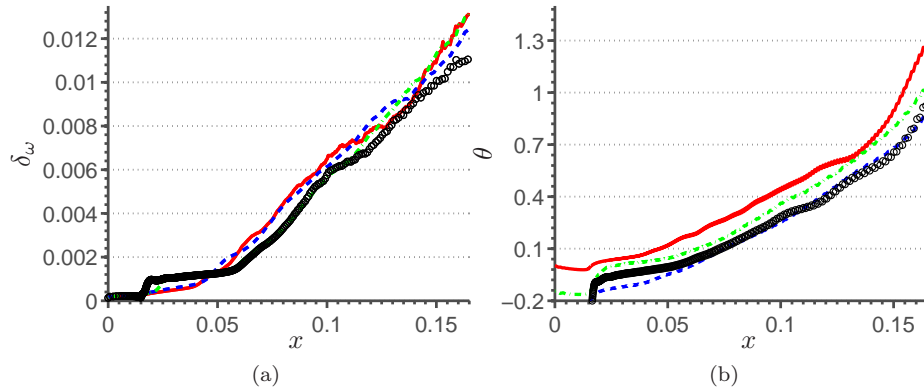


Figure 4.18: Vorticity and momentum thickness comparison between cases. — : B1; - - - : B2; . . . : B3; ooo: B4

Moreover, observing the pressure magnitudes for the mid-plane (Figure 4.19) also confirms that all the cases are getting similar in properties down-stream of the domain. In parallel, vorticity diagram in this plane also have a similar behavior which commences from the middle of the domain, the vorticity reduces in magnitude (lower velocity gradients) toward zero amount. All above-mentioned are signs of a turbulent behavior downstream of the domain.

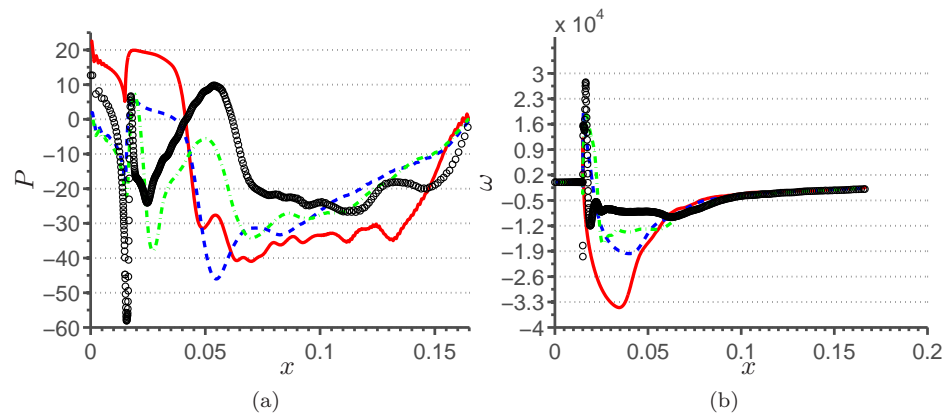


Figure 4.19: Vorticity and pressure of the mid-plane that crosses through the middle of plates for different cases. — : B1; - - - : B2; . . . : B3; ooo: B4

One more interesting thing to notice is the differences of case B1 to other

cases. Higher momentum thickness at the end of the domain, higher vorticity magnitude, and high fluctuation magnitudes are of this discrepancies. Although these differences are not large and also not in contradiction with the expectations, they show that in addition to the plate thickness, coarsening the grid has effects on the bulk evolution of the mixing layer. Logically, a coarse mesh cannot capture the small-scales of motion that is fixed firmly with coherent structures. On the other hand, large scales containing Kelvin-Helmholtz vortices are unaffected from changes in the mesh sizing.

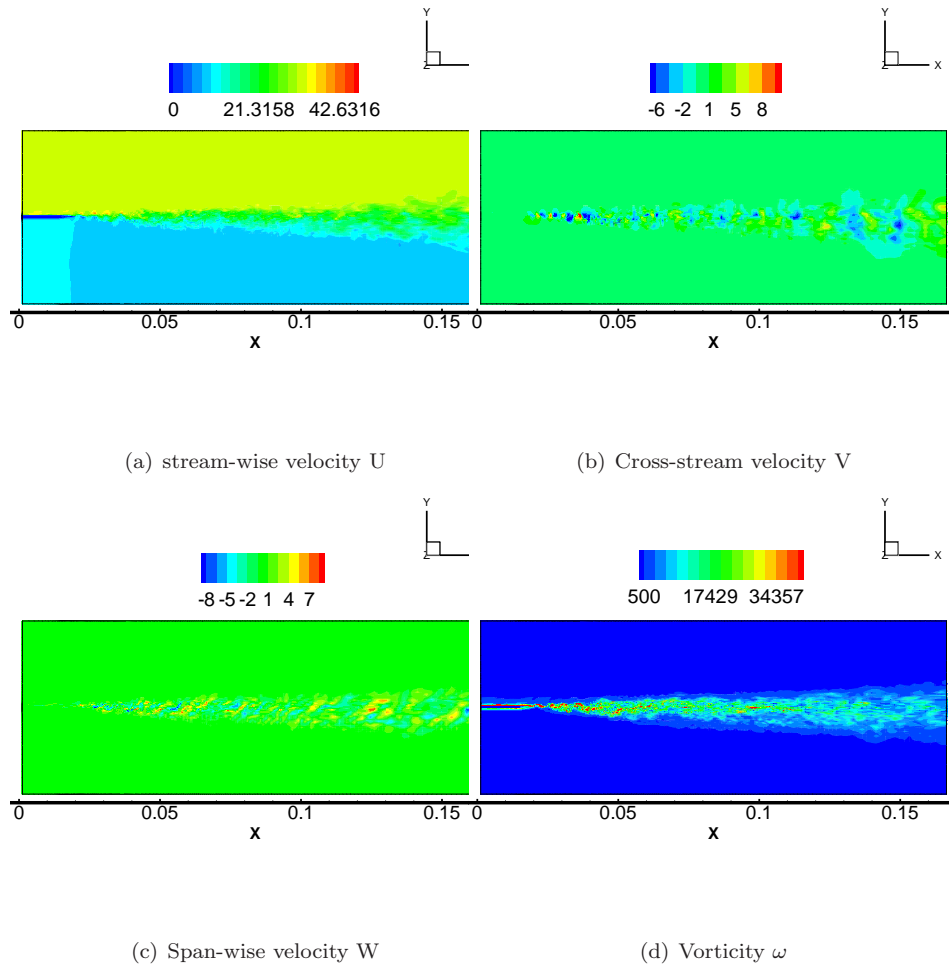


Figure 4.20: Instantaneous properties of the 3D case B6.

Take a look at the 3D instantaneous properties of case B6 at Figure 4.20. Comparing the results with the 3D hyperbolic tangent inlet profile shows a clear difference in length of the primary vortex sheet at the inlet. The effects of the plate in terms of igniting the mixing and the instabilities make the emergence of vortices possible much earlier than the preliminary simulations. Also, a big change in the vorticity contour of the shear layer is observable, in contrast with previous simulations, a more uniform distribution is detected before the

commencement of transition. The appearance of these scales happens simultaneously with pairing of primary vortices [9]. The most realistic way of finding the transition location is to look at the instantaneous vorticity plot and find the triggering place of amalgamation in a series of time steps and then time average. It is observed that the location is oscillating in the stream-wise direction. For instance, at *Figure 4.20*, the transition happens at $x \simeq 0.0075m$ with the corresponding Reynolds number of 11742 which is in consistency with Dimotakis' [26] investigations introducing a range of Reynolds numbers between 10000-20000 for commencement of transition. Finally, the transition is accomplished with creation of second pairings between span-wise vortices [9].

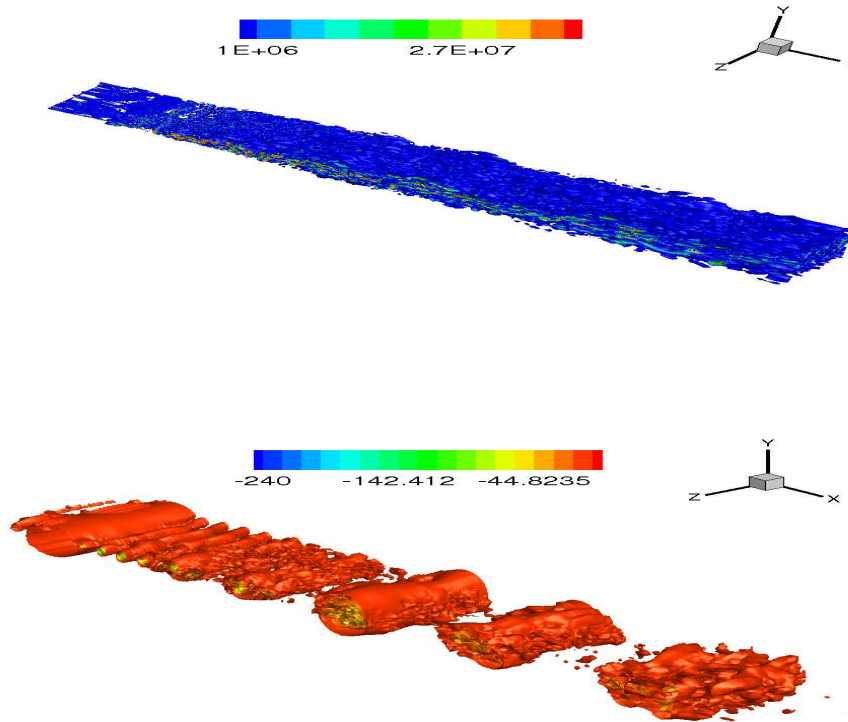


Figure 4.20: Small and large length scales' iso surfaces of case B6, respectively.

Small scales normally exist in the whole mixing layer, they are created from large scales through Cascade process and they vanish by transferring all their energy to heat through the dissipation term. These scales have a comparably small length compared to large and medium scales, which means they are rotating very fast, having high positive Q values. Overall, the magnitude of Q is lower downstream due to the reduction in gradients and vorticity in that area. See the uniformly distributed small scales at *Figure 4.20* and also the large scales in which the vortex sheet at the trailing edge of the plate and the first and second roll-up of the K-H vortices are clearly observable.

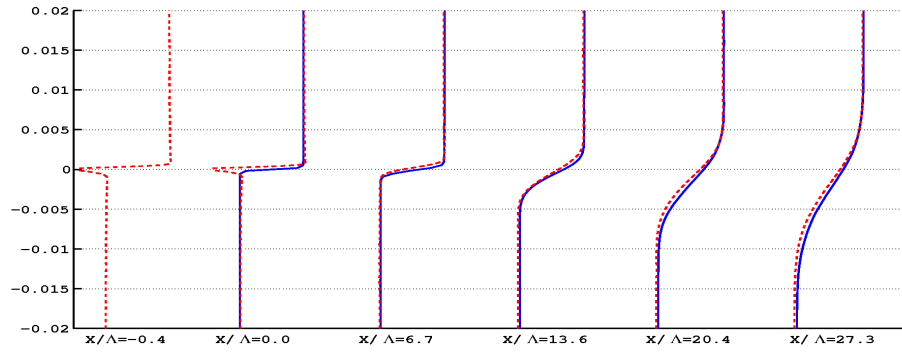


Figure 4.21: Comparison of the velocity profile in different cross-sections of the domain between preliminary and main simulations (A3 and B1).

Figure 4.21 demonstrates both preliminary and main results' time-averaged stream-wise velocity profiles along the domain. Large differences at the trailing edge exist. Downstream, both profiles look more like the same except that higher vorticity growth rate is visible in the main simulations.

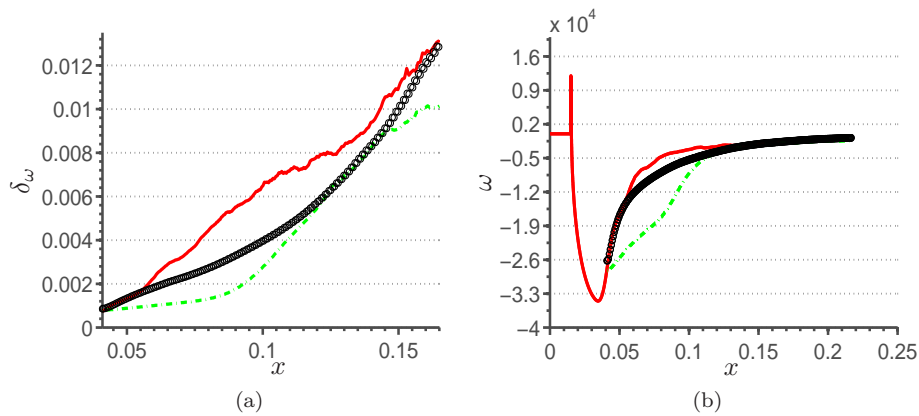


Figure 4.22: Vorticity thickness and vorticity at the mid-plane comparison between preliminary and main simulations with the same inlet velocities. --- : A3in2D; ooo: A3in3D; — : B1in2D

Due to the limited research time and the fact that recording sufficient time-averaged data from the 3D case take a long time and is currently in process, the preliminary simulations are only compared with case B1 which is in 2D. As it can be seen in Figure 4.22, the growth of the mixing layer in B1 case is faster and more linear compared to both 2D and 3D cases of preliminary simulations. That has a basis on the rise of instabilities in the flow which happens literally for case B1 and artificially for preliminary cases, respectively. Also, the vorticity diagram of the mid-plane shows similarities between case B1 and the 3D preliminary case with differences in pre-transition and transitional area ($Re = 7000 - 16000$) which is the area affected by the inlet conditions and the most important section for analysis of differences. It can be concluded that every case regardless of their inlet boundary condition when become fully de-

veloped turbulent, show a lot of similarities that brings the fact that turbulence condition is negligibly affected by the inlet conditions and is mostly a function of flow properties.

4.3.2 Comparison of turbulent models

Although the Smagorinsky model is well-known for its wide-range commercial and research applications, a number of studies found that with various setup and configurations of a case, the proper value for the Smagorinsky constant (C_S) could vary. This might bring concern in mind that in a transitional flow where the state of the flow alters rapidly, using a constant could bring up errors to the calculations. This and the use of an artificial damping function is the reason behind the simulations of the section. Here, case *B6* is simulated once with Smagorinsky model using the constant of 0.12 as it is used for all other cases of this report and another attempt is made with WALE model.

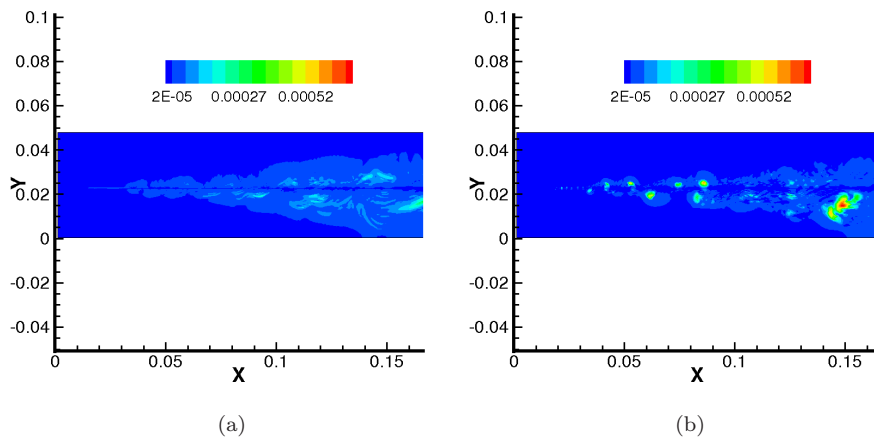


Figure 4.23: Instantaneous viscosity contours of case *B5* performed with the use of Smagorinsky model and WALE model, respectively.

Figure 4.23 demonstrates the viscosity magnitude contour for both cases. It can be seen that the WALE is capable of tuning the viscosity with the wall automatically. Since the pictures are taken in different time steps, they should not match together completely, therefore cannot be compared directly, but they have acceptable similarities in magnitude and area of effect. Comparing the time averaged properties of both cases also show a difference of less than 5% which can be considered negligible. Figure 4.24 compares the vorticity thickness of both cases. The vorticity thickness in the case using WALE model is slightly bigger than the other due to the fact that using constant Smagorinsky may result into over prediction of viscosity in some spots. Regardless of these differences which can also have an origin in other sources, it can be said that there are no considerable differences between the results of the models that can be of concern about the results of the project.

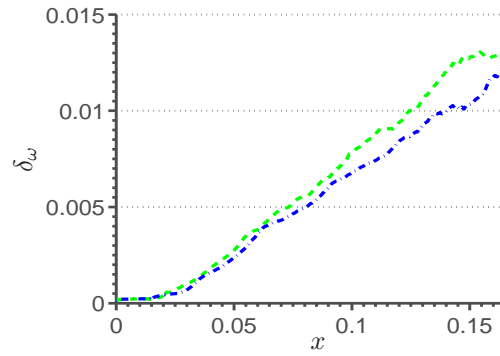


Figure 4.24: Comparison of the vorticity thickness between two models. - - - : WALE; — : Smagorinsky

This comparison has been carried out in 2D which might not be accurate enough to rely on for 3D cases. Time limits have hindered the author to perform such investigations and this can be considered as a future job. Although, it has been investigated that the evolution of the flow is largely unaffected by the use of Smagorinsky, Germano and Lilly or structure function model [13].

Chapter 5

Conclusion

5.1 Summary

IN this inquiry, several simulations are performed to provide information about planar mixing layers and the behavior of the flow in transition to turbulence inside shear layers. LES simulations are vastly used for investigations of mixing layers. The LES method can predict the behavior of the flow sufficiently accurate compared to DNS and experiments in much lower costs. Studies of this investigation of preliminary simulations agrees well with previous researches which can be a sort of verification for the results of the main section. 2D results using hyperbolic tangent profile provide poor predictions of the behavior of the flow compared to experiments. It seems that at those cases the flow stays in an unsteady laminar state instead of moving forward to a transition to turbulence.

In 3D cases, better results comparable to experiments have been obtained and a lot of discussions about different scales and the growth of the shear layer are presented in *Section 4.1* which indicates the importance of this setup. Comparing the preliminary results with the main results show that the transition location in simulations with hyperbolic tangent function as the inlet boundary profile is delayed but with a lower Reynolds number. That is also a sign of smaller growth of the layer compared to the main simulations with the splitter involved. Also, more concentrated vortex sheets are detectable near the trailing edge of the preliminary simulations specially in 2D cases.

Using a Blasius boundary layer profile together with the presence a splitter plate inside the domain provides more realistic results. Considerable differences near the trailing edge of the plate in terms of recirculating flows and the bubble, higher perturbations which change the growth pattern in the mixing layer and a change in the location of transition are of the properties that cannot be detected through using artificial inlet velocity profiles downstream of the trailing edge. Yet, it seems that all the cases downstream when the flow starts to become fully developed turbulent have similar properties and that shows the dependency of turbulence in mixing on the flow properties rather than the inlet condition and perturbations.

5.2 Future work

Since the time-span of the project is limited, investigations on 3D cases with the plate inside the domain is limited to instantaneous results of case B6. 3D simulations with different velocity ratios and different thicknesses of the plate can be performed and time-averaged results of the simulations can provide much more in terms of understanding the behavior of the mixing layer and the transitional area with respect to the splitter. The splitter plate is considered rectangular whereas it can have a curved profile instead to reduce the effects of the plate. Different shapes and more realistic plates with respect to the application of the mixing layer can be simulated.

Also, the same investigations can be carried out for the turbulent mixing layers with turbulent inlet profiles and also more investigations on the effect of forcing on the shear layer is a pertinent issue to follow.

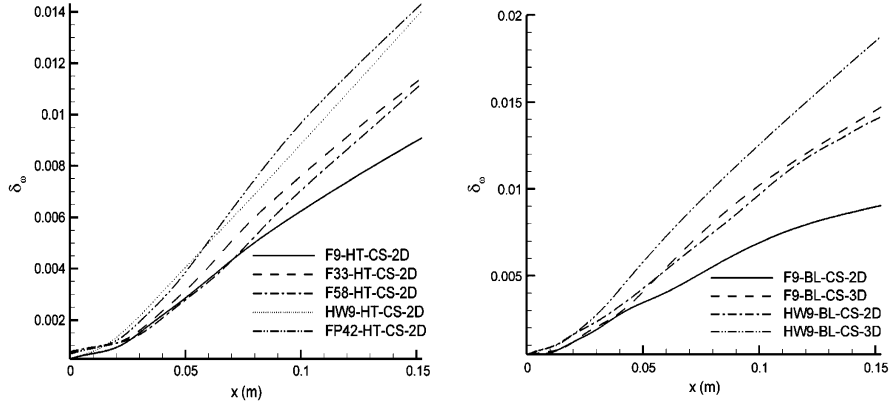
Appendices

Appendix A

Here, some of the results of McMullan *et al's* [13] research about mixing layers are brought up in order to be compared with the results of this project in Section 4. Table A.1 shows the setup information of different cases they have simulated. *HT* is used to show hyperbolic tangent inlet profile and *BL* expresses the Blasius boundary layer profile.

Table A.1: setup information for their different simulated cases.

experiment number	$U_1(ms^{-1})$	$U_2(ms^{-1})$	R	Δt
F9	31.39	12.96	0.42	1.2
F33	28.46	9.68	0.49	1.5
F58	19.93	6.81	0.49	1.6
HW9	32.12	9.59	0.54	1.2
FP42	21.58	5.19	0.61	1.6



(a) Two-dimensional boundary layer inflow condition simulations. (b) Cases F9-BL-3D, HW9-BL-3D, and their two-dimensional counterpart simulations.

Figure A.1: Vorticity thickness of different cases in 2D and 3D.

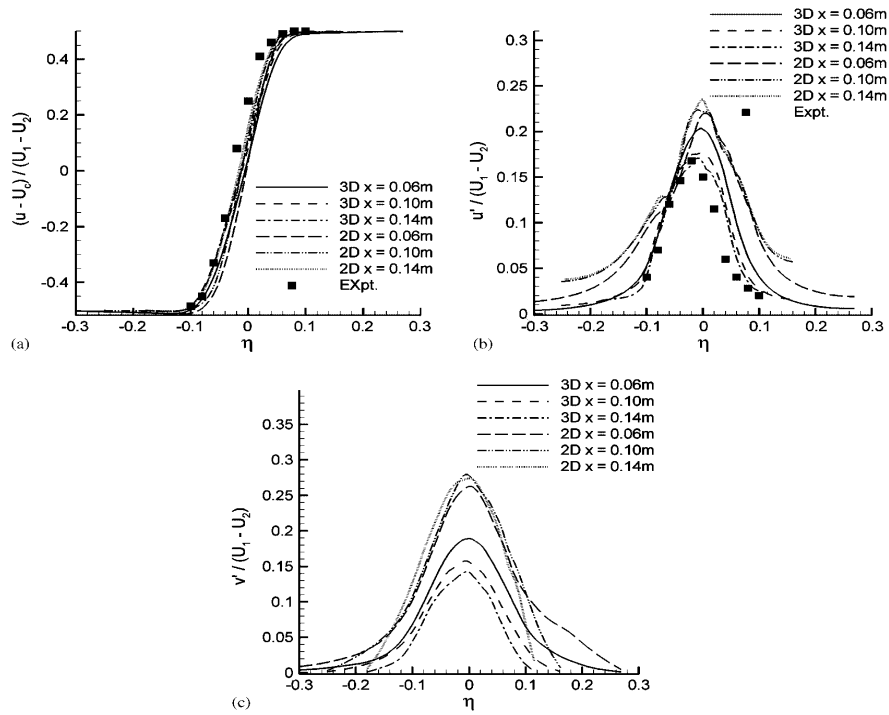


Figure A.2: Mean and RMS fluctuation velocity profiles for cases HW9-BL-2D and HW9-BL-3D.

Bibliography

- [1] Maghrebi M and Zarghami A. DNS of forced mixing layer. *International journal of numerical analysis and modeling*, 7:173–193, 2010.
- [2] Liepmann H. and Laufer J. Investigation of free turbulent mixing. *NASA TN*, 1257, 1947.
- [3] Brown G. and Roshko A. On density effects and large structure in turbulent mixing layer. *Fluid Mech*, 764:775–816, 1974.
- [4] Mungal M.G and Dimotakis P.E. Mixing and combustion with low release in a turbulent shear layer. *Fluid Mech*, 148:349–382, 1984.
- [5] Li Q. and Fu S. Numerical simulation of high-speed planar mixing layer. *Computers and Fluids*, 32:1357–1377, 2003.
- [6] Luo X. Hu Zh. and Luo K.H. Numerical simulation of particle dispersion in a spatially developing mixing layer. *Theoretical and Computational Fluid Dynamics*, 15:403–420, 2002.
- [7] Sada K. Michioka T., Kurose R. and M H. Direct numerical simulation of a particle-laden mixing layer with a chemical reaction. *international Journal of Multiphase Flow*, 31:843–866, 2005.
- [8] Madnia C.K. Miller R.S. and Givi P. Structure of a turbulent reacting mixing layer. *Combustion Science and Technology*, 99:1–36, 1994.
- [9] Gao S. McMullan W.A. and Coats C.M. The effect of inflow conditions on the transition to turbulence in large eddy simulations of spatially developing mixing layers. *International Journal of Heat and Fluid Flow*, 30:1054–1066, 2009.
- [10] Winant C.D. and Browand F.K. Vortex pairing: the mechanism of turbulent mixing layer growth at moderate reynolds numbers. *Fluid Mech*, 63:225–237, 1974.
- [11] Huang L. and Ho C. Small scale transition in a plane mixing layer. *Fluid Mech*, 210:475–500, 1990.
- [12] Parezanovic V. Mixing layer visualization. <http://berndnoack.com/news.php>, 2012.

- [13] Gao S. McMullan W.A. and Coats C.M. A comparative study of inflow conditions for two-and three-dimensional spatially developing mixing layers using large eddy simulation. *International Journal of Numerical Methods in Fluids*, 55:589–610, 2007.
- [14] Tanahashi M. Wang Y. and Miyauchi T. Coherent fine scale eddies in turbulence transition of spatially-developing mixing layer. *Heat Fluid Flow*, 28:1280–1290, 2007.
- [15] D’Ovidio A. Coherent structures in turbulent mixing layers. *PhD thesis, University of Leicester*, 1988.
- [16] Batt R.G. Some measurements on the effect of tripping the two-dimensional shear layer. *AIAA*, 13:245–247, 1975.
- [17] Davidson L. and Peng S.H. Hybrid les-rans: A one-equation SGS model combined with a k-omega model for predicting recirculating flows. *Int. J. Num. Meth. in Fluids*, 43:1003–1018, 2003.
- [18] Wikipedia. <http://en.wikipedia.org>. Large Eddy Simulation, 2013.
- [19] F. Nicoud and F. Ducros. Subgrid-scale stress modeling based on the square of the velocity gradient tensor.flow. *Turbulence, and Combustion*, 62:183–200, 1999.
- [20] Konrad JH. An experimental investigation of mixing in two-dimensional shear flows with applications to diffusion limited chemical reactions. *PhD thesis, California Institute of Technology, California*, 1976.
- [21] HUERRE P. <http://catalogue.polytechnique.fr/cours.php?id=2880&type=site>. CNRS-cole Polytechnique, 2011.
- [22] Ho C.M. and Huerre P. Perturbed free shear layers. *Fluid Mech*, 16:365–422, 1984.
- [23] Prandtl L. Uber flussigkeitsbewegung bei sehr kleiner reibung. *Proceedings of the third international mathematics congress*, pages 91–484, 1904.
- [24] Wygnanski I. and Feidler H.E. The two-dimensional mixing region. *J.Fluid Mech*, 41:327–361, 1970.
- [25] Johansson P. A three-dimensional laminar multigrid method applied to the simplec algorithm. *PhD thesis, Chalmers University of Technology, Sweden*, 1992.
- [26] Dimotakis P.E. The mixing transition in turbulent flows. *Fluid Mech*, 409:69–98, 2000.
- [27] Tanahashi M. Miyauchi T. and Suzuki M. Inflow and outflow boundary conditions for direct numerical simulations. *JSME*, 39:305–314, 1996.
- [28] Monkewitz P.A. and Heurre P. Influence of the velocity ratio on the spatial instability of mixing layers. *Phys. Fluids*, 25:1137–1143, 1982.
- [29] White F. Fluid mechanics, third edition, 1994.

-
- [30] Huang L. and Ho CM. Small scale transition in a plane mixing layer. *Journal of Fluid Mechanics*, 210:475–500, 1990.
- [31] Sondergaard R. Soria J. and Cantwell B.J. A study of the fine-scale motions of incompressible time-developing mixing layers. *Phys. Fluids*, 6:871–884, 1994.
- [32] Spencer B.W. Jones B.G. Statistical investigation of pressure and velocity fields in the turbulent two-stream mixing layer. *A.I.A.A.*, 1:71–613, 1971.